AFRL-RX-WP-TP-2009-4159

THE ROLE OF MICROSTRUCTURAL VARIABILITY ON THE VERY HIGH-CYCLE FATIGUE BEHAVIOR OF DISCONTINUOUSLY-REINFORCED ALUMINUM METAL MATRIX COMPOSITES USING ULTRASONIC FATIGUE (PREPRINT)

J.E. Spowart, J. Huang, and J.W. Jones

Metals Branch
Metals, Ceramics and NDE Division

MAY 2008

AIR FORCE RESEARCH LABORATORY
MATERIALS AND MANUFACTURING DIRECTORATE
WRIGHT-PATTERSON AIR FORCE BASE, OH 45433-7750
AIR FORCE MATERIEL COMMAND
UNITED STATES AIR FORCE

REPORT DOCUMENTATION PAGE

Form Approved
OMB No. 0704-0188

1. REPORT DATE *(DD-MM-YY)*	2. REPORT TYPE	3. DATES COVERED *(From - To)*
May 2008	Journal Article Preprint	01 May 2008 – 01 May 2008

4. TITLE AND SUBTITLE
THE ROLE OF MICROSTRUCTURAL VARIABILITY ON THE VERY HIGH-CYCLE FATIGUE BEHAVIOR OF DISCONTINUOUSLY-REINFORCED ALUMINUM METAL MATRIX COMPOSITES USING ULTRASONIC FATIGUE (PREPRINT)

5a. CONTRACT NUMBER
IN-HOUSE

5b. GRANT NUMBER

5c. PROGRAM ELEMENT NUMBER
62102F

6. AUTHOR(S)
J.E. Spowart (AFRL/RXLMD)
J. Huang and J.W. Jones (University of Michigan)

5d. PROJECT NUMBER
4347

5e. TASK NUMBER
RG

5f. WORK UNIT NUMBER
M02R4000

7. PERFORMING ORGANIZATION NAME(S) AND ADDRESS(ES)

Metals Branch (RXLMD)
Metals, Ceramics and NDE Division
Materials and Manufacturing Directorate
Wright-Patterson Air Force Base, OH 45433-7750
Air Force Materiel Command, United States Air Force

Department of Materials Science and Engineering
University of Michigan
Ann Arbor, MI

8. PERFORMING ORGANIZATION REPORT NUMBER
AFRL-RX-WP-TP-2009-4159

9. SPONSORING/MONITORING AGENCY NAME(S) AND ADDRESS(ES)
Air Force Research Laboratory
Materials and Manufacturing Directorate
Wright-Patterson Air Force Base, OH 45433-7750
Air Force Materiel Command
United States Air Force

10. SPONSORING/MONITORING AGENCY ACRONYM(S)
AFRL/RXLMD

11. SPONSORING/MONITORING AGENCY REPORT NUMBER(S)
AFRL-RX-WP-TP-2009-4159

12. DISTRIBUTION/AVAILABILITY STATEMENT
Approved for public release; distribution unlimited.

13. SUPPLEMENTARY NOTES
Submitted to International Journal of Fatigue
PAO Case Number and clearance date: WPAFB 08-2957, 17 April 2008.
The U.S. Government is joint author of this work and has the right to use, modify, reproduce, release, perform, display, or disclose the work.

14. ABSTRACT
The fatigue behavior of two 2009/SiC/15p-T4 DRA composites has been investigated in the very high cycle fatigue regime using ultrasonic fatigue to achieve the very high cycle counts. One composits displayed a very homogeneous spatial distribution with minimal particle clustering and the other displayed a relatively heterogeneous distribution with significant particle clustering. Fatigue cracks initiated almost exclusivley at A1CuFe inclusions in the homogeneous material and no crack initiation was observed at SiC particle clusters. Conversely, fatigue cracks initiated almost exclusively at clusters of SiC particles oin the herterogeneous material and no crack initiation at inclusions was observed. Fatigue lives in both compositers approaching 10 to the 9^{th} cycles exhibited minimal variation in lifetime and subsurface crack initiation was observed in all cases. Differences in the crack initiation behavior between the two composites were attributed primarily to variations in the spatial distribution of the reinformcement phase.

15. SUBJECT TERMS
high-cycle fatigue, variability, aluminum, ultrasonic fatigue, metal matrix composites

16. SECURITY CLASSIFICATION OF:			17. LIMITATION OF ABSTRACT:	18. NUMBER OF PAGES	19a. NAME OF RESPONSIBLE PERSON (Monitor)
a. REPORT	b. ABSTRACT	c. THIS PAGE			Daniel B. Miracle
Unclassified	Unclassified	Unclassified	SAR	56	19b. TELEPHONE NUMBER *(Include Area Code)* N/A

The Role of Microstructural Variability on the Very High-Cycle Fatigue Behavior of Discontinuously-Reinforced Aluminum Metal Matrix Composites Using Ultrasonic Fatigue

J. Huang[1], J.E. Spowart[2†], J.W. Jones[1]

[2]Air Force Research Laboratory, Materials and Manufacturing Directorate,
AFRL/RXLMD, Wright-Patterson AFB, OH

[1]Department of Materials Science and Engineering,
University of Michigan, Ann Arbor, MI

Abstract

The fatigue behavior of two 2009/SiC/15p-T4 DRA composites has been investigated in the very high cycle fatigue regime (VHCF, $10^7 \leq N_f \leq 10^9$ cycles) using ultrasonic fatigue to achieve the very high cycle counts. One composite displayed a very homogeneous spatial distribution with minimal particle clustering and the other displayed a relatively heterogeneous distribution with significant particle clustering. Fatigue cracks initiated almost exclusively at AlCuFe inclusions in the homogeneous material and no crack initiation was observed at SiC particle clusters. Conversely, fatigue cracks initiated almost exclusively at clusters of SiC particles in the heterogeneous material and no crack initiation at inclusions was observed. Fatigue lives in both composites approaching 10^9 cycles exhibited minimal variation in lifetime and subsurface crack initiation was observed in all cases. Differences in the crack initiation behavior between the two composites were attributed primarily to variations in the spatial distribution of the reinforcement phase.

† Corresponding Author: Jonathan E. Spowart (Jonathan.Spowart@wpafb.af.mil)

1. Introduction

Composite materials are increasingly gaining favor in the aerospace and transportation industries as designers strive to reduce component and system weights while still fulfilling structural requirements[1,2]. As compared to their monolithic counterparts, discontinuously-reinforced aluminum (DRA) composites generally display higher specific stiffness[3], greater specific strength[4], increased resistance to wear and creep[5-7], and improved high-cycle fatigue behavior[8-11] while still retaining good ductility and fracture toughness. Additionally, they are more easily processed using conventional techniques, such as extrusion and forging[12], and their properties are more isotropic than continuously-reinforced composites. These attributes make DRA materials excellent candidates for high-performance structural applications, particularly when combined with their low density. Many of these composite components are subjected to cyclic and/or vibrational loading and it is critical to understand the fatigue behavior of these materials in order to maximize their performance and reliability.

DRA composites have not been thoroughly investigated in the VHCF regime but extensive studies have been performed in the HCF regime. These studies were reviewed by Allison and Jones[13] and more recently by Llorca[14] and Chawla[15]. The improved high-cycle fatigue resistance of DRA composites as compared to their monolithic counterparts has been largely attributed to the ability of the material to effectively transfer load from the relatively weak matrix material to a stiffer and higher-strength reinforcement phase. However, microstructural heterogeneities in these materials that disrupt the efficiency or uniformity of this load transfer can serve as stress concentrators at which fatigue damage may accumulate, resulting in crack initiation. These heterogeneities can be a key factor in determining overall fatigue life, since crack initiation life, N_i, can comprise over 90% of the total fatigue life, N_f, at these longer lifetimes. In previous HCF studies on DRA materials, microstructural heterogeneities related to the reinforcement phase, such as particle clusters or abnormally large individual particles, have been shown to initiate fatigue cracks[8-11]. Fatigue cracks have also been observed to initiate at other microstructural features such as pores and intermetallic inclusions[8,9,11]. However, higher

volume fractions of reinforcement particles were also found to carry a larger percentage of applied load and, therefore, provided some shielding effect to these matrix heterogeneities[10]**Error! Bookmark not defined.**. In general, these studies suggest that DRA composites with a more homogeneous spatial distribution of reinforcements and a reduced number density of pores and intermetallics tend to display improved fatigue properties over those with a more heterogeneous distribution and greater number of matrix defects, especially at longer lifetimes.

Fatigue life prediction in the VHCF regime has become increasingly important as industry seeks to extract increasingly longer usable service lives while maintaining adequate safety factors. However, fatigue is typically a stochastic process where single microstructural "events" can play a critical role in dictating the overall fatigue life, particularly in the initiation-dominated longer-life regimes[16]. This variable nature can produce large amounts of scatter in fatigue life, making accurate fatigue predictions difficult. Traditional fatigue prediction models typically treat this variability in fatigue life in a statistical fashion where distribution functions are assigned, often resulting in overly conservative predictions at longer lifetimes that are necessary to meet typical safety factor requirements[17]. Therefore, the classically defined fatigue limit or fatigue strength as determined from HCF data may not adequately describe the fatigue behavior at these long lifetimes[18,19] making it necessary to investigate and understand the VHCF behavior of these materials experimentally. In comparison to statistically-based models, probability-based prediction methods that directly account for microstructural variability have potential to significantly increase predictive capabilities over their statistically-based counterparts[20-22].

The fatigue behavior of several important structural materials has been investigated in the VHCF regime, including steels[23-26], aluminum alloys[27,28] , nickel-based superalloys[29], and titanium alloys[30,31]. Ultrasonic fatigue has been shown in these studies to provide an accurate and reliable means of rapidly acquiring fatigue data in the gigacycle regime with largely insignificant effects of frequency on fatigue behavior, particularly in structural materials for which environmental attack does not play a key role in the fatigue process.

Interestingly, finite fatigue lifetimes have been recorded in the gigacycle regime for steels[23-26], which were previously characterized by a fatigue limit, below which fatigue life was considered infinite. Conversely, fatigue limits have been recorded for aluminum alloys[27,28], which were previously thought to have finite fatigue strengths even at very low applied stresses.

At these very long lifetimes, fatigue cracks have been primarily found to initiate subsurface at relatively low number density defects such as microshrinkage pores[27,28,32,33], large grains or clusters of grains[30,31], non-metallic inclusions[23,26] and intermetallic particles[34]. The dominance of these low number density microstructural heterogeneities in initiating fatigue damage was highlighted in a study by Yang et al[35] which investigated the fatigue behavior of "zero-inclusion" steels in which the inclusions present were not large enough to initiate fatigue cracks. These alloys displayed significantly longer fatigue lives as compared to commercially processed alloys that were of otherwise identical chemical compositions. Cracks initiated at the specimen surface either from the matrix or from machining artifacts in the "zero-inclusion" alloy rather than at subsurface defects.

Subsurface crack initiation has become a defining feature of the VHCF regime. Mughrabi[36] hypothesized that defects causing crack initiation in the VHCF regime must be present in sufficiently low number density such that they are not likely to exist at the specimen surface since surface-initiated cracks would normally be expected to propagate to critical size faster than subsurface ones due to their higher stress intensity for a given crack size. These internally initiated cracks will grow to critical size only if their propagation lifetime is shorter than the lifetime required for other damage accumulation processes to initiate a surface crack and then propagate it to failure.

In addition to representing an increasingly important class of structural materials, DRA composites are excellent model materials for studying the relationship between microstructural variability and fatigue behavior, due mainly to the ability to vary the spatial distribution of reinforcement particles via controlled processing. Bhanu-Prasad et al.[37] conducted a systematic study of PM-processed 2124/SiC/30p aluminum composites

in which matrix alloy powder particle sizes were increased, whilst maintaining a constant reinforcement particle size, thereby increasing the particle size ratio, or PSR. The SiC particles were found to congregate in the interstices of the larger matrix alloy powder particles, resulting in a more heterogeneous reinforcement distribution with increasing PSR, and larger variations in local area fractions of SiC particles as depicted schematically in Figure 1. The ultimate tensilestrengths and ductilities of the composites both decreased with increasing PSR. This was attributed to more effective load transfer from the matrix phase to a more homogeneously distributed reinforcement phase. A similar relationship between PSR and reinforcement distribution homogeneity in PM-processed AlCuMn/SiC/15p composites was also observed by Slipenyuk et al[38].

Several researchers have shown that extrusion improves the reinforcement particle spatial distribution with relatively minor particle orientation and banding effects[39-41]. In general, particle clustering was significantly reduced at higher extrusion ratios, yielding more spatially homogeneous particle distributions[42]. Larger particles and particles located in clusters were preferentially fractured during subsequent tensile loading, often skewing the post-extrusion particle size distributions towards smaller sizes. Yield strengths and ultimate tensile strengths are generally found to increase in the extruded samples, compared with vacuum hot-pressed (VHP) materials[43].

A variety of quantitative microstructural descriptors have been used by researchers to draw correlations between mechanical properties and microstructural features in spatially-heterogeneous systems such as DRA composites. These include analyses based on Dirichlet and other tessellations[44-49], inter-particle spacings[50-52], radial distribution functions[53], and *n*-point correlation functions[54,55]. However, these analysis schemes only interrogate the microstructure at the length scale of roughly the reinforcement particle size, and so are not as sensitive to microstructure beyond this. Tensile failure and fatigue behavior are controlled by multiple mechanisms operating on different length scales and, therefore, a multiple length scale analysis is required. More recently, the Multi-Scalar Analysis of Area Fractions (MSAAF) technique was developed by Spowart et al[56] to quantify the spatial homogeneity of DRA microstructures by measuring the variability of

local area fractions in a two-dimensional section[57,58]. Although a multi-scalar analysis, this technique can be used to yield a single scalar parameter – the *Homogeneous Length Scale*, L_H – which has units of length and represents the microstructural length scale beyond which the microstructure is homogeneous to within a defined range, commonly taken to be 0.01 (i.e. 1%). This technique has previously shown good sensitivity to spatial heterogeneity in DRA materials that have been deliberately processed to achieve different levels of reinforcement particle clustering[59]. Strong correlations were found between the 1% homogeneous length scale ($L_H^{1\%}$) and the measured tensile elongations of DRA specimens[58]. It is possible that even stronger correlations exist for fatigue properties, due to the highly localized nature of the deformation mechanisms occurring during fatigue loading.

The objective of the current study was to investigate the fatigue behavior of two DRA composites that were carefully processed to be nearly identical in composition but differing primarily in spatial distribution of SiC particles in order to examine the effects of microstructural variability on fatigue behavior. The present study builds on our previously-published work[34] on very high cycle fatigue behavior of a composite with a homogeneous SiC particle distribution, obtained via deformation (extrusion) processing. Both studies focused on the VHCF regime where crack initiation tends to be the main determining factor in overall fatigue life.

2. Materials

Three individual billets of 2009/SiC/15p-T4 aluminum metal matrix composite were produced for this study by DWA Aluminum Composites, Inc. using powder metallurgy techniques. Aluminum, magnesium, and copper powders were blended with 15 vol.% FEPA F-1000 grit silicon carbide particles. The blended powders were vacuum hot pressed (subsolidus) and then extruded to yield a fully-dense product. Composition of the 2009 matrix alloy was carefully controlled from billet to billet to ensure near-identical compositions. The matrix composition for each billet heat used in this study is listed in

Table 1. All three billets (I, II, and III) were extruded at a 14:1 extrusion ratio to yield a 97 mm diameter cylinder. Billets I and II were then subsequently re-extruded to yield a 16 mm diameter rod with a final extrusion ratio of approximately 404:1. All materials were solution heat-treated at 554°C and naturally aged (T4) for 96 hours prior to machining and testing. The mechanical properties of the individual composite specimens relative to the unreinforced matrix alloy are presented in Table 2.

3. Experimental procedure

3.1 Microstructural characterization

Metallographic specimens were sectioned in both transverse and longitudinal planes using a diamond wafering saw. Sections were mounted in resin and manually polished using SiC paper and diamond abrasive solutions with a final polish using Buehler Masterprep 0.05μm alumina suspension. Polished sections were examined in an unetched condition using an Olympus PME3 inverted metallurgical microscope with a DP12 digital camera system, and a Philips XL30FEG scanning electron microscope. Chemical analysis was performed using an EDAX Phoenix XEDS system. In addition to the MSAAF analysis, a commercial digital image analysis package (Clemex Vision PE 3.5) was also used to characterize such features as reinforcement particle volume fraction, aspect ratio, and orientation relative to the extrusion direction.

Previous fractographic analyses of failed samples[34] emphasized the significance of characterizing the intermetallic inclusion populations of the tested DRA materials. Therefore, metallographically prepared sections of both sets of materials were systematically scanned for intermetallic inclusions using optical microscopy. Multiple transverse gage section surfaces were examined until at least 100 inclusions per extrusion ratio were recorded for statistical analysis. Inclusions were modeled as spherical particles for ease of analysis, with equivalent section diameters defined as the diameter of the smallest circle that could be circumscribed about each inclusion. The Schwartz-

Saltykov method[60] was applied to the two-dimensional inclusion data to determine the three-dimensional spherical particle size distributions for each material.

3.2 Fatigue

Ultrasonic fatigue techniques were used in this study to acquire data in the VHCF regime in a more practical timeframe than conventional techniques would normally allow. Test frequencies in this study were approximately 20 kHz, as compared to 20-40 Hz of standard fatigue methodologies. Details of the experimental setup for ultrasonic fatigue are described elsewhere[61,62]. Briefly, in this method, a piezoelectric transducer operating at approximately 20 kHz produces resonant vibration in a standard-sized fatigue specimen. Under resonant conditions, maximum displacement occurs at the specimen ends, while a condition of maximum strain exists in the center of the gage section. Applied stresses are calculated by converting strains imposed on the specimen using the material modulus of elasticity, and assuming elastic deformation of the specimen. The system is calibrated at low applied displacements using strain gages applied to the specimen center, augmented by displacement measurements made at test loads by high resolution, non-contacting optical instrumentation (MTI-2000 Fotonic Sensor) During fatigue cycling, the vibration amplitude at the specimen end is monitored using an induction-based vibration gage. This vibration gage delivers input to a closed electronic feedback loop that maintain constant applied strain amplitude during testing. Strain levels along the gage length vary by less than 5%.

Rods 16mm in diameter were trepanned from the 97mm 14:1 extrusion in the longitudinal direction using electrical discharge machining (EDM) in order to provide machining blanks with similar dimensions to the 404:1 materials prior to machining. Thirty ultrasonic fatigue samples of the 404:1 material and ten samples of the 14:1 materials were machined to the dimensions shown in Figure 2. Specimen gage sections were subjected to low-stress grinding and a three-step final polish using successively finer SiC papers to minimize surface residual stresses. Fatigue tests were performed

under fully reversed loading conditions (R = -1) at a frequency of approximately 20 kHz, at ambient temperature, in air. Applied stresses were calculated based on Young's modulus values measured by a resonant frequency technique[63]. During testing, fatigue loading was applied intermittently in a pulse/pause mode, and compressed air cooling was utilized continuously to minimize heating in the gage section. The specimen gage temperature was monitored during fatigue cycling using a Type K thermocouple, and was maintained below 30ºC at all times. Samples were cycled until resonant conditions could no longer be satisfied because of changes in specimen compliance resulting from fatigue crack growth or until 10^9 cycles were reached, at which point runouts were declared. Runout samples were subsequently retested at higher stress levels, until final failure occurred.

Ten fatigue specimens for conventional servohydraulic fatigue experiments were also machined from the 404:1 extrusion ratio material. Sample gage and shoulder dimensions were identical to the ultrasonic fatigue samples with only minimal modifications of the threads necessary to facilitate specimen mounting in the load train of an MTS Series 810 servohydraulic test frame. Specimen surface preparation was identical to that for the VHCF (ultrasonic) specimens. Stress-controlled axial fatigue tests were performed under fully reversed loading conditions at ambient temperature in air, at a frequency of 30 Hz with a sinusoidal waveform using a carefully aligned servo-hydraulic test system in order to provide a direct comparison with previous conventional fatigue data on similar materials. Samples were cycled to failure or to 10^7 cycles, at which point runouts were declared. Runout samples were retested at higher stress levels until final failure occurred.

3.4 Analysis of failed samples

The fracture surfaces of failed samples were examined using a Philips XL30FEG SEM to characterize crack initiation features and overall fracture surface morphology. An EDAX Phoenix XEDS system was used for both fractographic analysis and selected compositional mapping of failed samples. Matching fracture surfaces of selected samples

were examined to further document the crack initiation features. Manual serial cross-sectioning was also performed on selected samples to provide additional morphological information about initiation features.

4. Results

4.1 Microstructure

Reinforcement particle distribution and particle orientation relative to the extrusion direction for the 404:1 extruded material is shown in Figure 3. Multi-Scale Analysis of Area Fraction (MSAAF) analyses show relatively homogeneous particle distributions with L_H values of 300 µm and 1200 µm for transverse and longitudinal sections, respectively. Additional image analysis showed a random distribution of particle orientations in the transverse plane and a preferential particle orientation along the direction of extrusion in the longitudinal plane. The SiC particle size distribution is slightly bimodal as shown in Figure 4, with an average equivalent spherical diameter of 7.3 µm and a standard deviation of 3.8 µm. The average particle aspect ratio (as defined by the ratio of major to minor axis length for a best-fit ellipse for each particle) was approximately 2:1.

Reinforcement particle distribution and relative particle orientation for the 14:1 extruded material is shown in Figure 5. MSAAF analyses on the 14:1 extruded material reveal a significantly more heterogeneous reinforcement particle distribution with L_H values of 830 µm and 1900 µm for transverse and longitudinal sections, respectively. Particle orientations were also found to be random in the transverse plane and preferentially oriented in the direction of extrusion in the longitudinal plane, but significant particle clustering and banding effects were also observed. Measured SiC particle sizes displayed a wide distribution as shown in Figure 6, with an average equivalent spherical diameter of 5.4 µm (SD = 2.7 µm). As with the 404:1 extruded material, the average particle aspect ratio was approximately 2:1.

Optical microscopy of unetched metallographic cross sections revealed small intermetallic inclusions, as shown in Figure 7. The distributions of equivalent two-dimensional inclusion section diameters for both materials are shown in Figure 8. The population size distributions approximate to log-normal distributions, with mean section diameters of 7.6 μm and 7.2 μm and standard deviations of 3.3 μm and 5.9 μm for the 14:1 and 404:1 extruded materials, respectively. It should be noted that no two-dimensional inclusion diameters larger than 25 μm were observed in the 14:1 extruded material.

The calculated equivalent three-dimensional spherical section diameter distributions for both materials as determined using the Schwartz-Saltykov method[60] are shown in Figure 9. The three-dimensional population size distributions also roughly followed log-normal distributions with mean spherical diameters of 8.5 μm and 9.9 μm and standard deviations of 3.0 μm and 4.5 μm for the 14:1 and 404:1 extruded materials, respectively. Inclusions with diameters larger than approximately 20μm are predicted to be extremely rare.

4.2 Fatigue behavior

Although runouts are typically declared at 10^7 cycles in conventional fatigue tests, fatigue lifetimes approaching 10^9 cycles were measured experimentally in this study using ultrasonic fatigue methods. The VHCF results for both the 14:1 and 404:1 extruded DRA composites obtained using ultrasonic fatigue and HCF results at conventional frequencies for the 404:1 composite obtained in the present study are shown in Figure 10 along with HCF data from previous fatigue studies by other researchers on similar materials using conventional techniques[10,11]. The VHCF behavior of both DRA materials studied in this investigation are in good agreement with the trend for fatigue lifetimes established by the earlier HCF data obtained using conventional frequencies. Fatigue lifetimes determined at 30 Hz in the present work also agree well with these earlier results. Fatigue lifetimes at a given stress amplitude and extrusion ratio generally follow a narrow Weibull

distribution. Importantly, the VHCF behavior indicates very little variability in fatigue lifetime, with a total range of *less than one order of magnitude* at a given stress amplitude for each extrusion ratio, as shown in Figure 11. This contrasts sharply with previous VHCF studies on other structural materials, in which a large range of fatigue lifetime variability was observed[27-30]. The standard deviations for the 404:1 extruded material are 1.43 x 10^8 cycles and 1.63 x 10^8 cycles at stress amplitudes of 200 MPa and 175 MPa, respectively. Standard deviations for the 14:1 extruded material at a stress amplitude of 175 MPa are significantly lower, at 5.48 x 10^7 cycles, and this material also displays a slightly lower mean fatigue life, as confirmed by a "student-t" statistical test ($p = 0.03$).

4.3 Crack initiation

In the 404:1 extruded materials subjected to ultrasonic fatigue, all failures initiated subsurface and almost exclusively at similarly-sized intermetallic inclusions, having a mean diameter of approximately 40 μm[34], as shown in Figure 12. No fatigue failures were observed to initiate from either SiC particles or clusters of particles. From XEDS compositional mapping, the inclusions were identified as AlCuFe intermetallics as shown in Figure 13. Matching-half fractography suggests that many of these initiating inclusions had actually fractured prior to the application of cyclic stress. This pre-existing damage was observed both in the form of inclusions that have fractured and separated, leaving a void in between the two halves (Figure 14), and in the form of inclusions that have fractured but not separated. In both cases, the damage to these brittle inclusions is unlikely to have occurred during fatigue loading given the low cyclic stress amplitudes applied in the VHCF regime, between 175 MPa and 200MPa.

All VHCF failures in the 14:1 extruded material also initiated exclusively at subsurface features. However, in contrast to the 404:1 extruded material, nearly all fatigue crack initiation occurred at *clusters* of SiC particles. No fatigue cracks were observed to initiate at the intermetallic inclusions present in this material. SiC clusters from which the critical fatigue cracks initiated were similar in size, with a mean width of

approximately 100 µm as shown in Figure 15. Initiating SiC clusters displayed complete matrix infiltration in most cases with unwetted particles observed at the initiation site in only one specimen.

In contrast to the VHCF results, all fatigue failures in the 404:1 extruded materials tested using conventional fatigue techniques initiated at the specimen surface, as shown in Figure 16. No initiation at SiC clusters was observed and single initiation sites were located randomly with respect to sample orientation in the load train. Initiation at surface-located AlCuFe inclusions similar to those found to initiate fatigue cracks in the same material using ultrasonic fatigue was noted in only two cases, and three initiation sites displayed no identifiable microstructural feature. The remaining failures were attributed to surface defects presumably resulting from specimen surface preparation. These initiation sites were associated with large longitudinal surface gouges and/or pits remaining from SiC particles that may have been inadvertently extracted during the finishing process. In some instances, it appears that a SiC particle may also have been redeposited into the sample surface as shown in Figure 17. Whether the origin of this particle is from the polishing papers or from the SiC reinforcement itself is unclear.

4.4 Crack propagation

Crack growth in the area immediately surrounding the initiation site is extremely tortuous for both materials tested in the VHCF regime using ultrasonic fatigue, as shown in Figure 18. However, the region of high tortuosity is more highly defined in the 404:1 extruded material than in the 14:1 extruded material. Outside of this region, crack growth continues radially in a direction nominally perpendicular to the tensile axis then abruptly becomes sharply angled in all failed samples as shown in Figure 19. Crack surface morphology is noticeably rougher in the 14:1 extruded material suggesting more prominent deflection of the crack tip. Stress intensities for these very short cracks are very low and may produce much slower crack growth rates due to increased crack tip deflection as it interacts with microstructural features such as individual SiC particles

and/or clusters of SiC particles. This region of high tortuosity was not observed at the initiation site in the 404:1 extruded material tested in the HCF regime using conventional fatigue techniques.

Decohered and/or fractured SiC particles are not observed on any of the fracture surfaces obtained for either material near the initiation site, but are visible near the transition from fatigue crack growth to fracture, as shown in Figure 20. This is consistent with the findings of Hall et al[11] and suggests that the fatigue crack propagates primarily through the matrix until ΔK values are sufficiently high that particles are surrounded by the plastic zone ahead of the crack tip.

5. Discussion

The processing of the DRA composites examined in this study was carefully controlled so as to vary only the spatial heterogeneity of the SiC reinforcement phase. Matrix alloy powder chemistry was precisely monitored and all processing steps, including heat treatment, were identical for all materials investigated. However, significant differences in the spatial distribution of SiC particles were produced by using intentional variations in extrusion ratio. The highly extruded 404:1 material used in this study displayed a very homogeneous reinforcement distribution with minimal clustering of particles. In contrast, the 14:1 extruded material displayed a markedly more heterogeneous SiC particle distribution and significant particle clustering and banding was observed as shown in Figure 21. Interestingly, the mean particle diameter in the 404:1 extruded material was observed to be slightly larger than that of the 14:1 extruded material at 7.3 μm vs 5.4 μm, but this difference may be attributable to typical batch-to-batch variations. In addition, the SiC particle size distribution of both materials also has a wide distribution, with standard deviations of 3.8 μm and 2.7 μm for the 404:1 and 14:1 materials, respectively. To simplify the subsequent analysis, the mean diameters are assumed to be roughly identical.

In the 404:1 extruded material, fatigue cracks initiated almost exclusively at relatively mono-sized intermetallic inclusions having a diameter of approximately 40 μm and no fatigue cracks were observed to initiate at either large individual SiC particles or clusters of particles. Both of these reinforcement-related microstructural features have been demonstrated to initiate fatigue cracks in previous HCF studies on similar DRA materials[8-11]. However, neither of these features were observed in optical metallographic sections and the MSAAF analysis of the spatial distribution of reinforcement particles in the 404:1 extruded material suggests a low number density of particle clusters. In general, the reinforcement phase was observed to have minimal overall effect on crack initiation in this material and the highly homogeneous reinforcement distribution highlighted the existing intermetallic inclusions as the dominant stress concentrator leading to fatigue damage.

Conversely, fatigue cracks initiated almost exclusively at relatively mono-sized clusters of SiC particles in the 14:1 extruded DRA composite. Accordingly, particle clusters of varying sizes and extensive particle banding were commonly observed in optical metallographic sections, and the MSAAF analysis quantifiably confirmed that the particles were relatively heterogeneously distributed with significant amounts of particle clustering. Additionally, those particle clusters observed to initiate fatigue cracks in the 14:1 extruded material were larger than the inclusions observed to initiate fatigue cracks in the 404:1 extruded material by roughly a factor of two, with a maximum size of approximately 100 μm. It is reasonable that the higher density population of large clusters presents a higher probability of initiating fatigue cracks at reinforcement-related microstructural features, as compared to the 404:1 extruded material. A rough order-of-magnitude estimate can be made directly from the MSAAF analysis, by assuming that the *local* volume fraction of SiC inside the cluster is around 50%. This is reasonable when compared to the global volume fraction of 15% (see also Figure 21). The order-of-magnitude probability of locating an area with a local volume fraction of 50% and of size of ~100 μm is around 10^{-6} for the 14:1 extruded material. This translates into a number per unit volume of around $10^{7}m^{-3}$.

Although intermetallic inclusions were observed to initiate fatigue cracks only in the 404:1 extruded materials, similar inclusions were observed in both extruded materials, using optical metallography. The mean equivalent spherical diameters of inclusions observed in both DRA composites (as predicted by the Schwartz-Saltykov method) are similar, with the 404:1 extruded material displaying a slightly larger mean inclusion diameter of approximately 9.9 μm (σ = 4.5 μm) as compared to 8.5 μm (σ = 3.0 μm) for the 14:1 extruded material. However, inclusions that were observed to initiate fatigue cracks in the 404:1 material were more than 6σ from the mean, approximately 40-50 μm in diameter. Therefore, it is extremely challenging to accurately predict the number density of these critical inclusions, even using extreme value statistics. However, even if it assumed that the 14:1 extruded materials contain the same size distribution of critical inclusions, pre-existing damage such as fractured and/or separated inclusions observed at the crack initiation sites in the 404:1 extruded materials was not observed in the 14:1 extruded materials, presumably due to the lower extrusion ratio. However, even if it is assumed that a similar population of pre-damaged inclusions is present in the 14:1 extruded material, their effect on crack initiation is negligible, since the presence of the ~100μm SiC clusters apparently favors crack initiation at these microstructural features rather than at intermetallic inclusions, either with or without any pre-existing damage. In general, these results for the 14:1 extruded material are reminiscent of the "zero inclusion"' steels studied by Yang et al[35]. In the present case, crack intitiation at the SiC clusters is favored over the inclusions. This can be attributed to their relatively large size and relative ease of propagating a crack within the cluster.

The pre-existing damage observed in those inclusions which initiated fatigue cracks in the 404:1 extruded materials may also help explain the very low scatter in the fatigue lives at each given stress amplitude. Fatigue initiation is normally expected to dominate the overall fatigue life, N_f, at longer lifetimes The stochastic nature of crack initiation would typically result in increasing scatter with increasing lifetimes, as crack initiation lifetime, N_i, would tend to be highly variable. If this damage was assumed to be a pre-existing crack with a crack size equivalent to the size of the inclusion diameter, the crack initiation lifetime would be negligible. The overall fatigue life is then dependent solely

on the more deterministic crack propagation lifetime, N_p. This fact, coupled with the almost mono-size distribution of initiating inclusions, is the likely cause of the unusually small amount of scatter in lifetimes measured in the VHCF regime.

The reduced scatter in the lifetime data of the 14:1 extruded DRA material also suggests that the overall fatigue life is similarly dominated by the crack propagation lifetime rather than initiation lifetime. Pre-existing damage was generally not observed in the 14:1 extruded material, however, clusters of SiC particles similar in size to the initiating clusters, but from which cracks did not initiate, were observed in random metallographic sections. This suggests that either the initiating clusters may have possessed pre-existing damage that was not readily observable, or that fatigue damage accumulates very rapidly in the clusters. As in the 404:1 extruded material, the initiating features in the 14:1 extruded material were also mono-sized, with the SiC clusters having a maximum size of approximately 100 μm. If the initial crack size, a_i, is assumed to be equal to the diameter of the initiating cluster, then a_i in the 14:1 extrued material is roughly twice that of the 404:1 extruded material. Along with the mono-sized nature of the initiating clusters, this serves not only to reduce the scatter in the fatigue lifetimes of the 14:1 extruded material, but also to reduce the mean lifetime, as compared to the 404:1 extruded material, at the same stress level.

Subsurface crack initiation was consistently observed in all specimens tested in the VHCF regime. Based on a spatial analysis of subsurface initiation by Mughrabi[64], the number of critical initiating features located at the specimen surface can be defined as:

$$N_{i,s} = n_i \cdot \pi \cdot d \cdot d_i \cdot l$$

where n_i is the volume density of critical initiating features of diameter d_i, in a cylindrical gage section with dimensions of $d \times l$. Since stress intensities of surface cracks are approximately $\sqrt{2}$ greater than internal cracks of equal length[65], it is reasonable to assume that no critical initiating features are located at the gage surface, since they would readily grow to critical size well before subsurface cracks. If the initiating inclusions in the

404:1 extruded materials and the initiating SiC *clusters* in the 14:1 extruded materials are both modeled as spherical defects with diameters of 40 μm and 100 μm, respectively, then n_i must be less than 1.03×10^{8} m^{-3} (for the inclusions) or 4.11×10^{7} m^{-3} (for the clusters) to satisfy the condition $N_{i,s} < 1$. This would evaluate to a very low number density of fewer than thirty-two inclusions of critical size in the gage section volume of the 404:1 extruded material, and less than twenty critically-sized SiC clusters in the gage section volume of the 14:1 extruded material, which is consistent with the rough estimates of number densities of clusters obtained from the MSAAF data.

The above analysis ignores the effects of any residual compressive stresses that may exist. Although the multi-stage low-stress grinding procedure used during specimen preparation should be effective in minimizing residual stresses, it does not eliminate them entirely. From previous experience, it is estimated that there still exists approximately 200-250 MPa of compressive stress at the sample surface although the residual stress condition was not measured experimentally in the current study. At the low stress amplitudes used in the present ultrasonic fatigue studies, there would essentially be no applied stresses at the gage surface and no surface initiation would be expected even if critically sized inclusions and/or SiC clusters were present. However, the stresses applied during the conventional HCF studies were well above the estimated compressive residual stress level. As such, the surface layer is expected to experience cyclic tensile stresses during testing, and experimental observations support this notion. Conventional fatigue tests of the 404:1 extruded materials resulted exclusively in surface-initiated failure, but primarily at surface defects associated with the sample fabrication procedure. Only a small percentage of conventional fatigue cracks were observed to initiate at AlCuFe inclusions similar to those found to initiate cracks in the (lower stress level) ultrasonic fatigue tests, and no crack initiation was observed at SiC clusters or large individual SiC particles. It is therefore reasonable to assert that residual compressive surface stresses may influence the location of fatigue crack initiation sites at lower stress levels and very long lifetimes, although microstructural features that are typically found to cause subsurface initiation are likely still relatively low number fraction.

6. Conclusions

The two DRA composites investigated in the current research can be viewed as model materials for studying the role of microstructural variability in the very high-cycle fatigue regime. Each material displays a distinct crack initiation feature that can be directly tied to quantifiable differences in microstructure. Both initiation mechanisms are present to some degree in each material, but the number fraction, size, and nature of those features relative to each other will determine which one will actually initiate fatigue cracks. In the spatially heterogeneous 14:1 extruded material, reinforcement particle clusters are significantly larger and produce higher stress concentrations than inclusions of critical size that may otherwise initiate damage. In the spatially homogeneous 404:1 extruded material, however, there is minimal clustering of the SiC. At the low applied stresses used in this study, this two-phase material behaves more like a monolithic material, since the homogeneous spatial distribution of the reinforcement enables efficient load transfer from the matrix to reinforcement particles, without producing stress concentrations sufficient to initiate fatigue cracks. The SiC reinforcement therefore has a minimal effect on crack initiation in the more homogeneous material, which allows the AlCuFe inclusions to emerge as the dominant initiation features.

Acknowledgements

The authors would like to acknowledge the following individuals for their valuable assistance in this work: Chris Torbet of the University of Michigan, and Cory Smith and Mark van den Bergh of DWA Aluminum Composites. This project was funded by the U.S. Air Force Office of Scientific Research (Grant No: F49620-03-1-0069), whose assistance is gratefully acknowledged.

References

[1] Miracle, DB, (2006). Aeronautical Applications of Metal Matrix Composites. In: *ASM Handbook, Vol. 2, Properties and Selection: Nonferrous Alloys and Special-Purpose Materials, 10th Ed.*, p. 1043-1049.

[2] Hunt, Jr., WH and Miracle, DB, (2006). Automotive Applications of Metal Matrix Composites. In: *ASM Handbook, Vol. 2, Properties and Selection: Nonferrous Alloys and Special-Purpose Materials, 10th Ed.*, p. 1029-1032.

[3] Miracle, DB (2005). Metal matrix composites – From science to technological significance, *Compos. Sci. Tech.*, 65, 2526-2540.

[4] Wu Y, Lavernia EJ (1992). Strengthening behavior of particulate reinforced MMCs. *Scr. Metall. Mater.*, **27**, 173-178.

[5] Wang A, Rack HJ (1991). Transition wear behavior of SiC-particulate- and SiC-whisker-reinforced 7091 Al metal matrix composites. *Mater. Sci. Eng. A, Struct. Mater. Prop. Microstruct. Process.,* **A147,** 211-224.

[6] Modi OP, Prasad BK, Yegneswaran AH, Vaidya ML (1992). Dry sliding wear behaviour of squeeze cast aluminum alloy-silicon carbide composites. *Mater. Sci. Eng. A, Struct. Mater. Prop. Microstruct. Process.,* **A151**, 235-245.

[7] Hong SH, Chung KH (1995). High temperature creep behavior of SiC/2124Al metal matrix composites. *Key Eng. Mat.,* **104-107**, 757-764.

[8] Bonnen JJ, Allison JE, Jones JW (1991). Fatigue behavior of a 2xxx series aluminum alloy reinforced with 15 vol pct SiC_p. *Metall. Trans. A,* **22A**, 1007-1019.

[9] Li C, Ellyin F (1996). Fatigue damage and its localization in particulate metal matrix composites. *Mater. Sci. Eng. A, Struct. Mater. Prop. Microstruct. Process.,* **A214,** 115-121.

[10] Chawla N, Andres C, Davis LC, Jones JW, Allison JE (2000). The interactive role of inclusions and SiC reinforcement on the high-cycle fatigue resistance of particle reinforced metal matrix composites. *Metall. Mater. Trans. A, Phys. Metall. Mater. Sci.,* **31A,** 951-957.

[11] Hall JN, Jones JW, Sachdev AK (1994). Particle size, volume fraction and matrix strength effects on fatigue behavior and partice fracture in 2124 aluminum-SiC_p composites. *Mater. Sci. Eng. A, Struct. Mater. Prop. Microstruct. Process.,* **A183**, 69-80.

[12] Hunt WH (2000). Aluminum metal matrix composites today. *Mater. Sci. Forum,* **331-337**, 71-84.

[13] Allison JE, Jones JW (1993). Fatigue behavior of discontinuously reinforced metal-matrix composites. In: *Fundamentals of Metal Matrix Composites* (Edited by Suresh S, Mortensen A, Needleman A). Butterworth-Heinemann, Boston, pp. 269-294.

[14] Llorca J (2002). Fatigue of particle- and whisker-reinforced metal-matrix composites. *Prog. Mater. Sci.*, **47**, 283-353.

[15] Chawla N, Shen YL (2001). Mechanical behavior of particle reinforced metal matrix composites. *Adv. Eng. Mater.*, **3**, 357-370.

[16] Laz PJ, Hillberry BM. Int. J. Fatigue 1998;20;263.

[17] Harlow DG, Wei RP. Key Eng. Mat. 2001;200;119.

[18] Marines I, Bin X, Bathias C (2003). An understanding of very high cycle fatigue of metals. *Int. J. Fatigue.*, **25**, 1101-1107.

[19] Bathias C, Bechet J (2003). Effect of microstructure on the very high cycle fatigue of alloy at room and cryogenic temperatures. In: *Materials Lifetime Science and Engineering.* TMS, Warrendale, PA, 51-58.

[20] Todinov MT. Mat. Sci. Eng. 1998;A255;117.

[21] Chan, KS. Met. Mat. Trans. 2003;34A;43.

[22] Boselli J, Pitcher PD, Gregson PJ, Sinclair I (2001). Numerical modeling of particle distribution effects on fatigue in Al-SiCp composites. *Mater. Sci. Eng. A, Struct. Mater. Prop. Microstruct. Process.*, **300**, 113-124.

[23] Wang QY, Berard JY, Dubarre A, Baudry G, Rathery S, Bathias C (1999). Gigacycle fatigue of ferrous alloys. *Fatigue Fract. Engng. Mater. Struct.*, **22**, 667-672.

[24] Wang QY, Bathias C, Kawagoishi N, Chen Q (2002). Effect of inclusion on subsurface crack initiation and gigacycle fatigue strength. *Int. J. Fatigue.*, **24**, 1269-1274.

[25] Murakami R, Yonekura D, Ni Z (2002). Fatigue fracture behavior of high-strength steel in super long life range. *JSME Int. J. Ser. A Solid Mech. Mater. Eng.*, **45**, 517-522.

[26] Murakami Y, Yokoyama NN, Nagata J (2002). Mechanism of fatigue failure in ultralong life regime. *Fatigue Fract. Eng. Mater. Struct.*, **25**, 735-746.

[27] Caton MJ, Jones JW, Mayer H, Stanzl-Tschegg S, Allison JE (2003). Demonstration of an endurance limit in cast 319 aluminum. *Metall. Mat. Trans. A Phys. Metall. Mat. Sci.*, **34A**, 33-41.

[28] Zhu X, Shyam A, Jones JW, Mayer H, Lasecki JV, Allison JE (2004). Effects of Microstructure and Temperature on Fatigue Behavior of E319-T7 Cast Aluminum Alloy in Very Long Life Cycles International Journal of Fatigue, 28 (2006) 1566-1571.

[29] Shyam A, Torbet CJ, Jha SK, Larsen JM, Caton MJ, Szczepanski CJ, Pollock TM, Jones JW (2004). Development of ultrasonic fatigue for rapid, high-temperature fatigue studies in turbine engine materials. In: *Superalloys 2004*. Edited by: Green KA, Pollock TM, Harada H, Howson TE, Reed RC, Schirra JJ, and Walston S. TMS, Warrendale, pp. 259-268.

[30] Ravi Chandran KS, Jha SK (2005). Duality of the S-N fatigue curve caused by competing failure modes in a titanium alloy and the role of Poisson defect statistics. *Acta Mater.*, **53**, 1867-1881.

[31] Bathias C, Bechet J (2003). Effect of microstructure on the very high cycle fatigue of alloy at room and cryogenic temperatures. In: *Materials Lifetime Science &*

Engineering. Edited by: Liaw PK, Buchanan RA, Klarstrom DL, Wei RP, Harlow DG, and Tortorelli PF. TMS, Warrendale, pp. 51-58.

[32] A Probabilistic Model of Fatigue Strength Controlled by Porosity Population in A 319-type cast Aluminum Alloy. Part I: Model Development, X. Zhu, J.Z. Yi, J.W. Jones and J.E. Allison, Metall. Mater. Trans. A, 38A(2007)1111-1123.

[33] A Probabilistic Model of Fatigue Strength Controlled by Porosity Population in A 319-type cast Aluminum Alloy Part II: Monte-Carlo Simulation J.Z. Yi, X. Zhu, J.W. Jones and J.E. Allison, Metall. Mater. Trans., 38A(2007)1123-1135.

[34] Huang, J, Spowart, JE, Jones, JW (2006). Fatigue Behavior of SiCp-reinforced aluminium composites in the very high cycle regime using ultrasonic fatigue. *Fatigue Fract. Engng. Mater. Struct.*, **29**, 507-517.

[35] Yang ZG, Li SX, Zhang JM, Zhang JF, Li GY, Li ZB, Hui WJ, Weng YQ (2004). The fatigue behaviors of zero-inclusion and commercial 42CrMo steels in the super-long fatigue life regime. *Acta Mater.*, **52**, 5235-5241.

[36] Mughrabi H (2002). On 'multi-scale' fatigue life diagrams and the relevant life-controlling mechanisms in ultrahigh-cycle fatigue. *Fatigue Fract. Eng. Mater. Sruct.,* **25**, 755-764.

[37] Prasad VVB, Bhat BVR, Mahajan YR, Ramakrishnan P (2002). Structure-property correlation in discontinuously reinforced aluminium matrix composites as a function of relative particle size ratio. *Mater. Sci. Eng. A, Struct. Mater. Prop. Microstruct. Process.*, **337**, 179-186.

[38] Slipenyuk A, Kuprin V, Milman Y, Spowart JE, Miracle DB (2004). The effect of matrix to reinforcement particle size ratio (PSR) on the microstructure and mechanical properties of a P/M processed AlCuMn/SiCp MMC. *Mater. Sci. Eng. A, Struct. Mater. Prop. Microstruct. Process.*, **381**, 165-170.

[39] Tham LM, Gupta M, Cheng L. Mat. Sci. Eng. A 2002;A326;355.

[40] Davies CHJ, Chen WC, Hawbolt EB, Samarasekera IV, Brimacombe JK. Scripta Met. Mat. 1995;32;309.

[41] Cöcen Ü, Önel K. Comp. Sci. Tech. 2002;62;275.

[42] Tan MJ, Zhang X. Mat. Sci. Eng. A 1998;244;80.

[43] Wilks GB, Influence of Reinforcement Homogeneity on the Deformation and Fracture of a Discontinuously Reinforced Aluminum Matrix Composite, Ph.D. thesis, Pennsylvania State University (2007).

[44] Murphy AM, Howard SJ, Clyne TW (1998). Characterization of severity of particle clustering and its effect on fracture of particulate MMCs. *Mater. Sci. Technol.*, **14**, 959-968.

[45] Stone IC, Tsakiropoulos P (1995).Characterisation of spatial distribution of reinforcement in powder metallurgy route Al/SiC_p metal matrix composites. Part 1-techniques based on microstructure. *Mater. Sci. Technol.*, **11**, 213-231.

[46] Everett RK, Geltmacher AB (1999). Spatial distribution of MnS inclusions in HY-100 steel. *Scripta Mater.*, **40**, 567-571.

[47] Lewandowski JJ, Liu C (1989). Effects of matrix microstructure and particle distribution on fracture of an aluminum metal matrix composite. *Mater. Sci. Eng. A, Struct. Mater. Prop. Microstruct. Process.*, **107**, 241-255.

[48] Bertram M, Wendrock H (1996). Characterization of planar local arrangement by means of the Delaunay neighbourhood. *J. Microsc.*, **181**, 45-53.

[49] Yang N, Boselli J, Gregson PJ, Sinclair I (2000). Simulation and quantitative assessment of finite-size particle distributions in metal matrix composites. *Mater. Sci. Technol.*, **16**, 797-805.

[50] Li M, Ghosh S, Richmond O, Weiland H, Rouns TN (1999). Three dimensional characterization and modeling of particle reinforced metal matrix composites. Part 1: Quantitative description of microstructural morphology. *Mater. Sci. Eng. A, Struct. Mater. Prop. Microstruct. Process.*, **256**, 153-173.

[51] Tewari A, Dighe M, Gokhale AM (1998). Quantitative characterization of spatial arrangement of micropores in cast microstructures. *Mater. Charact.*, **40**, 119-132.

[52] Tao S, Boyd JD (1993). Mechanisms of Damage Accumulation and Fracture in Particulate Reinforced Metal-Matrix Composites. In: *Proceedings of the ASM 1993 Materials Congress*. ASM International, Materials Park, OH, pp. 29-40.

[53] Louis P, Gokhale AM (1996). Computer simulation of spatial arrangement and connectivity of particles in three-dimensional microstructure: application to model electrical conductivity of polymer matrix composite. *Acta Mater.*, **44**, 1519-1528.

[54] Torquato S (1991). Random heterogeneous media. Microstructure and improved bounds on effective properties. *Appl. Mech. Rev.*, **44**, 37.

[55] Pyrz R (1994). Correlation of microstructure variability and local stress field in two-phase materials. *Mater. Sci. Eng. A, Struct. Mater. Prop. Microstruct. Process.*, **177**, 253-259.

[56] Spowart JE, Maruyama B, Miracle DB (2001). Mult-scale characterization of spatially heterogeneous systems: implications for discontinuously reinforced metal-matrix composite microstructures. *Mater. Sci. Eng. A, Struct. Mater. Prop. Microstruct. Process.*, **301**, 51-66.

[57] Spowart JE, Ma ZY, Mishra RS (2003). The effect of friction stir processing (FSP) on the spatial heterogeneity of discontinuously-reinforced aluminum (DRA) microstructures, in: *Friction Stir Welding and Processing II* (Edited by: Jata KV, Mahoney M, Mishra RS). TMS, Warrendale, pp. 243-252.

[58] Tewari A, Gokhale AM, Spowart JE, Miracle DB (2004). Quantitative characterization of spatial clustering in three-dimensional microstructures using two-point correlation functions. *Acta. Mater.*, **52**, 307-319.

[59] Tewari, A, Spowart, JE, Gokhale, AM, Mishra, R, Miracle, DB (2006). Characterization of the Effects of Friction Stir Processing on Microstructural Changes in DRA Composites. *Mat. Sci. Eng. (A)* **428**, 80-90.

[60] Underwood E (1970). *Quantitative Stereology*. Addison-Wesley Publishing Co., Reading.

[61] Mayer HR, Lipowsky HJ, Papakyriacou M, Roesch R, Stich A, Stanzl-Tschegg S (1999). Application of ultrasound for fatigue testing of lightweight alloys. *Fatigue Fract. Eng. Mater. Struct.*, **22**, 591-599.

[62] Shyam A, Torbet CJ, Jha SK, Larsen JM, Caton MJ, Szczepanski CJ, Pollock TM, Jones JW (2004). Development of ultrasonic fatigue for rapid, high temperature fatigue studies in turbine engine materials. In: *Superalloys 2004, Proceedings of the Tenth International Symposium on Superalloys.* TMS, Warrendale, PA, 259-268.

[63] Yu CJ, Prucher Y (1993). Measuring Young's modulus and shear modulus – a comparison of dynamic and mechanical techniques. *Adv. Powder Metall. Part. Mater.*, **1**, 273-286.

[64] Mughrabi H (2002). On 'multi-scale' fatigue life diagrams and the relevant life-controlling mechanisms in ultrahigh-cycle fatigue. *Fatigue Fract. Eng. Mater. Sruct.*, **25**, 755-764.

[65] Y. Murakami, Metal Fatigue: Effect of Small Defects and Nonmetallic Inclusions, Elsevier Science Ltd, Boston MA, 2002, p.369.

Tables:

Figures:

Figure 14: a) and b) Matching half SEM fractographs of typical initiation site in 404:1 extruded DRA composite material. c) SEM image of sample tilted at 60° showing void at inclusion fracture surface.

Figure 15: Secondary election and corresponding XEDS compositional maps identify initiation features in 14:1 extruded DRA materials as SiC clusters.

Figure 16: Macroscopic SEM image of fracture surface of 404:1 extruded DRA composite tilted at 45° and tested using conventional fatigue techniques at higher stress along with typical initiation site. σ_a = 300 MPa, $N_f = 1.69 \times 10^6$ cycles, R = -1, f = 30 Hz.

Figure 17: SEM image of conventional fatigue sample gage surface showing surface pit related to presence of large SiC particle or cluster of particles.

Figure 18: SEM images of 404:1 extruded and 14:1 extruded DRA composite fracture surfaces showing regions of tortuous crack growth at initiation site followed by region of crack growth nominally perpendicular to the tensile axis.

Figure 19: SEM image of 404:1 extruded DRA composite tilted at 45° showing typical fracture surface morphology. Crack initiation site is highlighted.

Figure 20: SEM images of fracture surfaces of both DRA composite materials at increasing radial distance from crack initiation site. SiC particles are not visible on the fracture surface in the region immediately surrounding the initiation site.

Figure 21: Optical image of large SiC cluster in metallographically-prepared transverse section of the 14:1 extruded DRA composite.

table_1

Extrusion Ratio	Billet heat	Cu (3.2-4.4)	Mg (1.0-1.6)	Si (<0.25)	Fe (<0.20)	Zn (<0.10)	O (<0.60)	Others, each (<0.05)	Others, total (<0.15)
404:1	I	4.12	1.33	0.12	0.11	<0.01	0.33	<0.05	<0.15
404:1	II	4.09	1.31	0.14	0.11	<0.01	0.40	<0.05	<0.15
14:1	IIII	4.00	1.30	0.12	0.13	0.01	0.32	<0.05	<0.15

† **DWA Aluminum Composites, Chatsworth, CA.**
Note: **Matrix chemistry is controlled by Forge de Bologne Material Specification CCM-01 – DRA 2009 SiC 15p**

table_2

Billet heat	E (GPa)		σ_u (MPa)		σ_y (MPa)		$\%e_f$	
	LT1	**LT2**	**LT1**	**LT2**	**LT1**	**LT2**	**LT1**	**LT2**
I	93.8	93.8	490.0	475.0	347.0	350.0	6.3	4.8
II	92.4	91.8	494.0	477.0	354.0	337.0	5.8	6.2
III	103.8	106.2	465.2	486.4	352.5	355.4	3.8	4.37

[†] DWA Aluminum Composites, Chatsworth, CA.

figure_01
Click here to download high resolution image

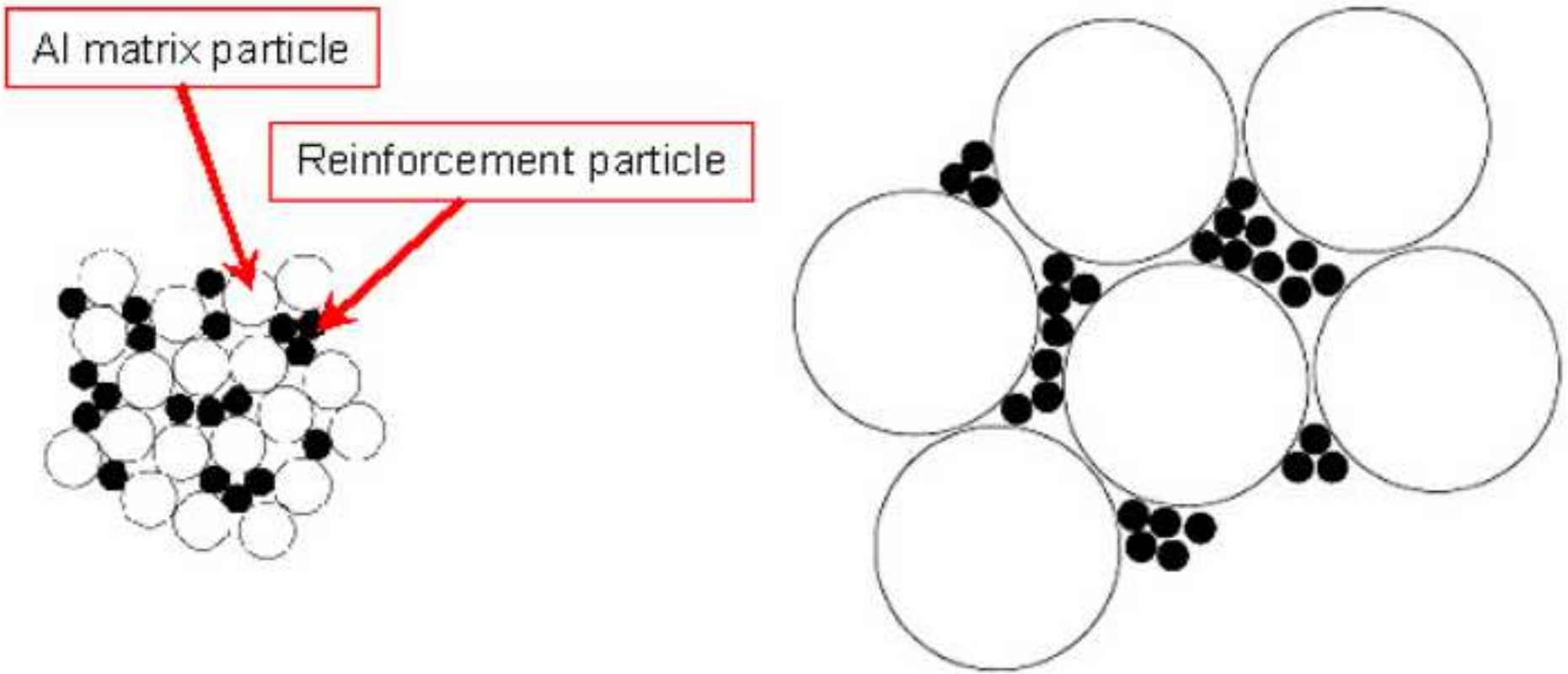

figure_02
Click here to download high resolution image

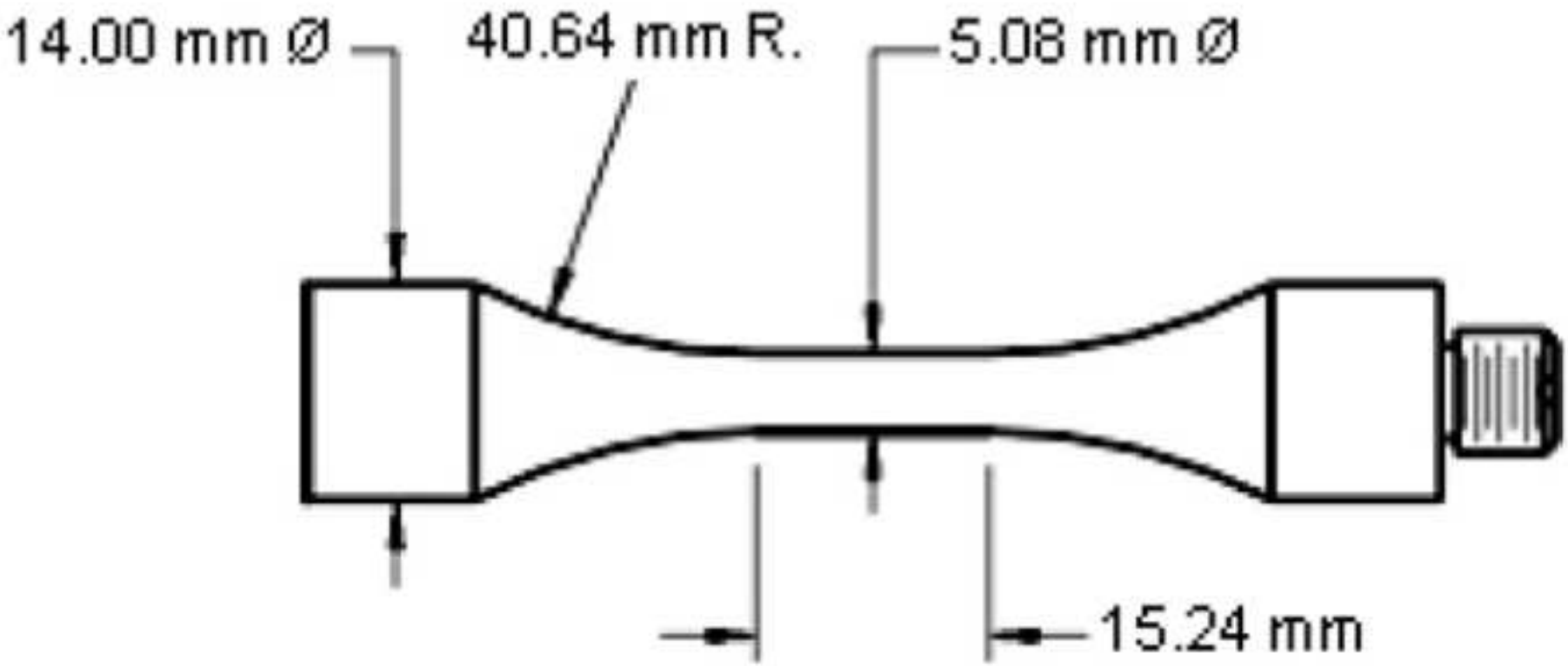

figure_03
Click here to download high resolution image

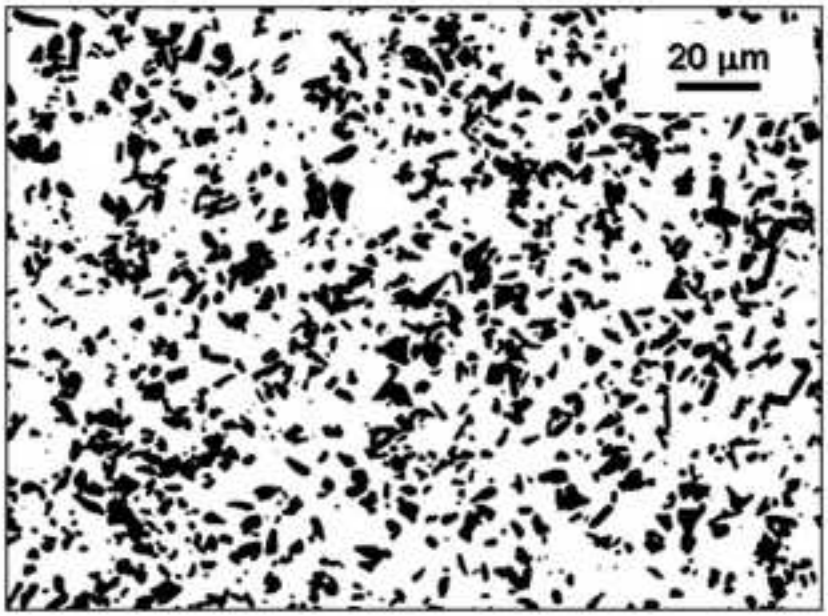

Transverse section

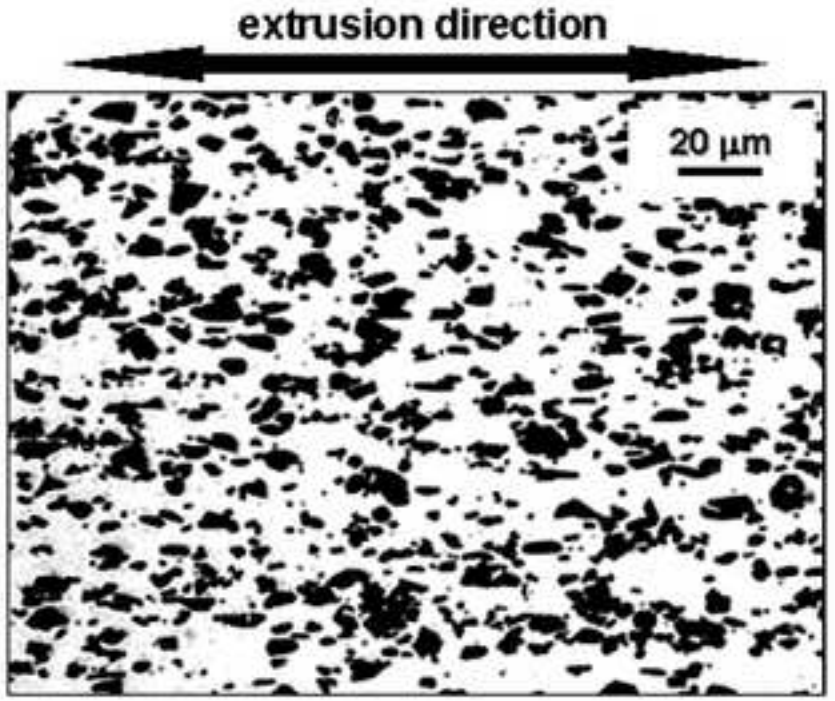

Longitudinal section

figure_04
Click here to download high resolution image

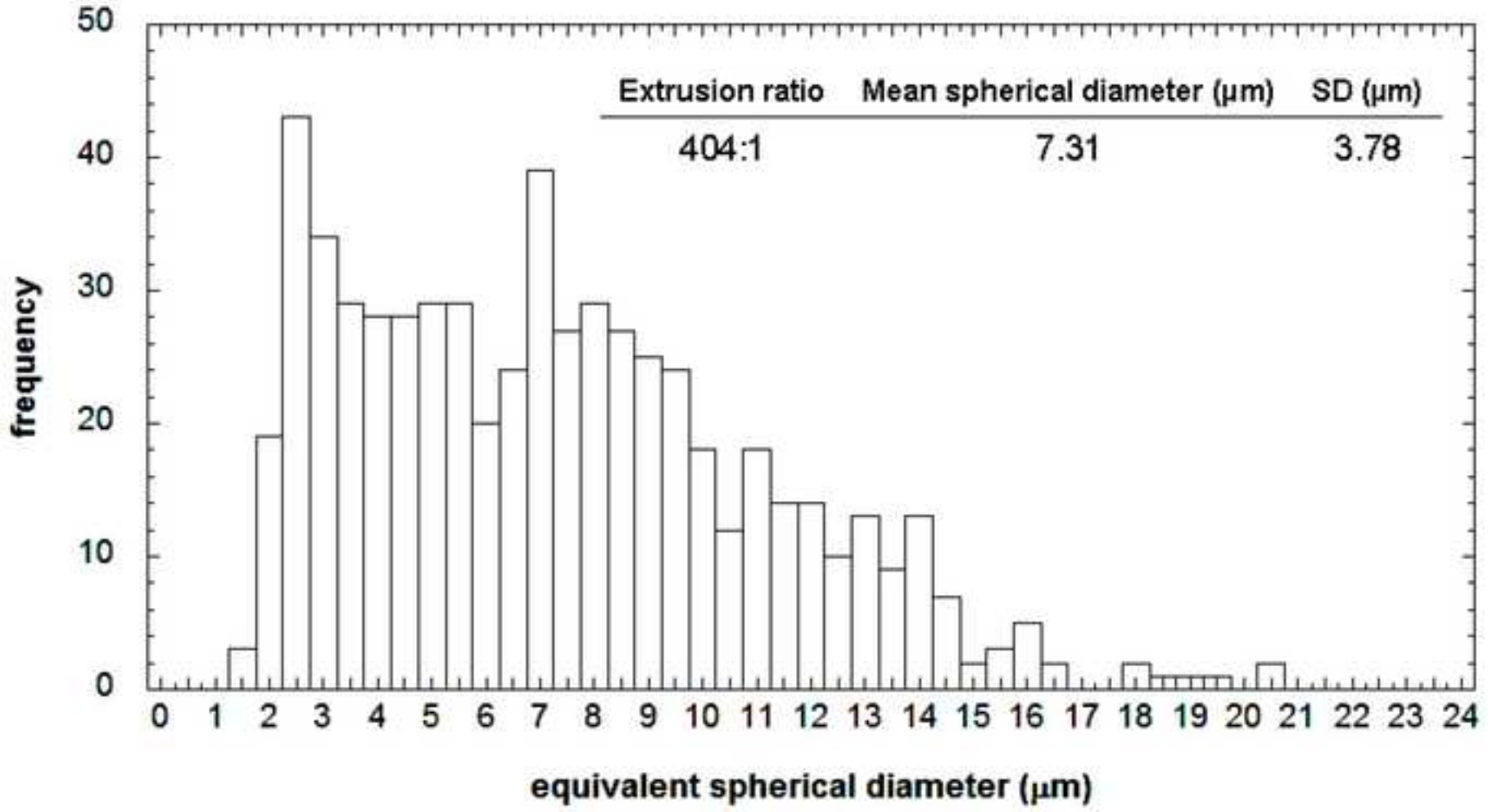

figure_05
Click here to download high resolution image

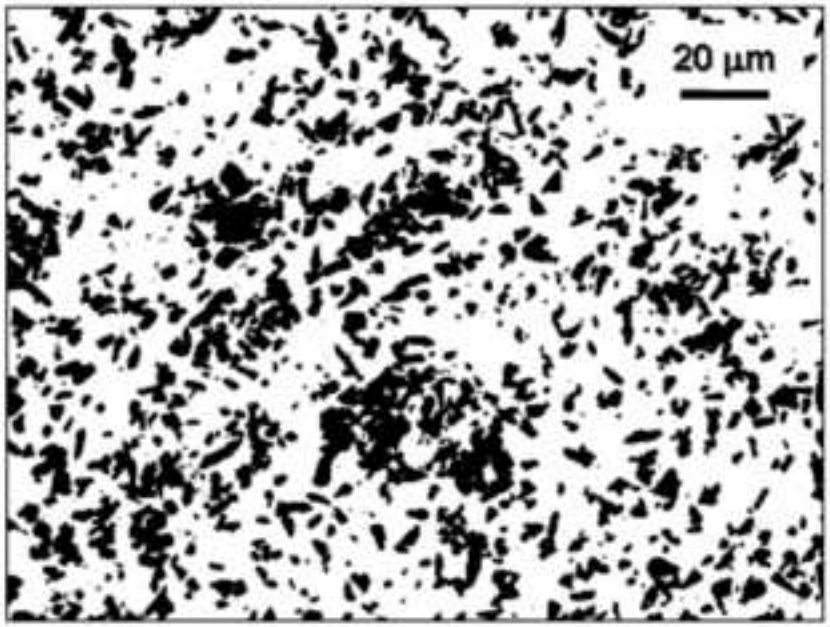

Transverse section

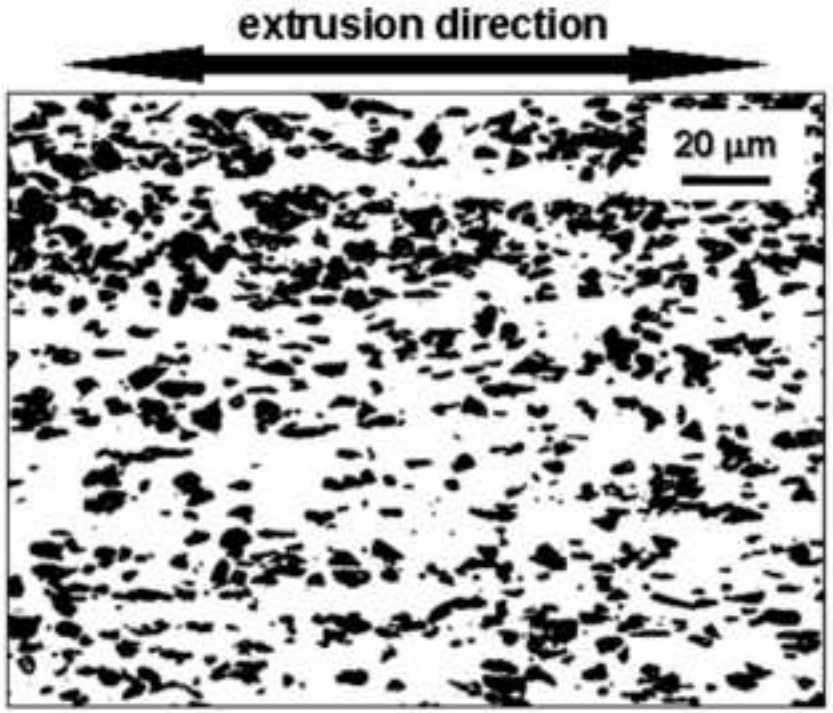

Longitudinal section

figure_06
Click here to download high resolution image

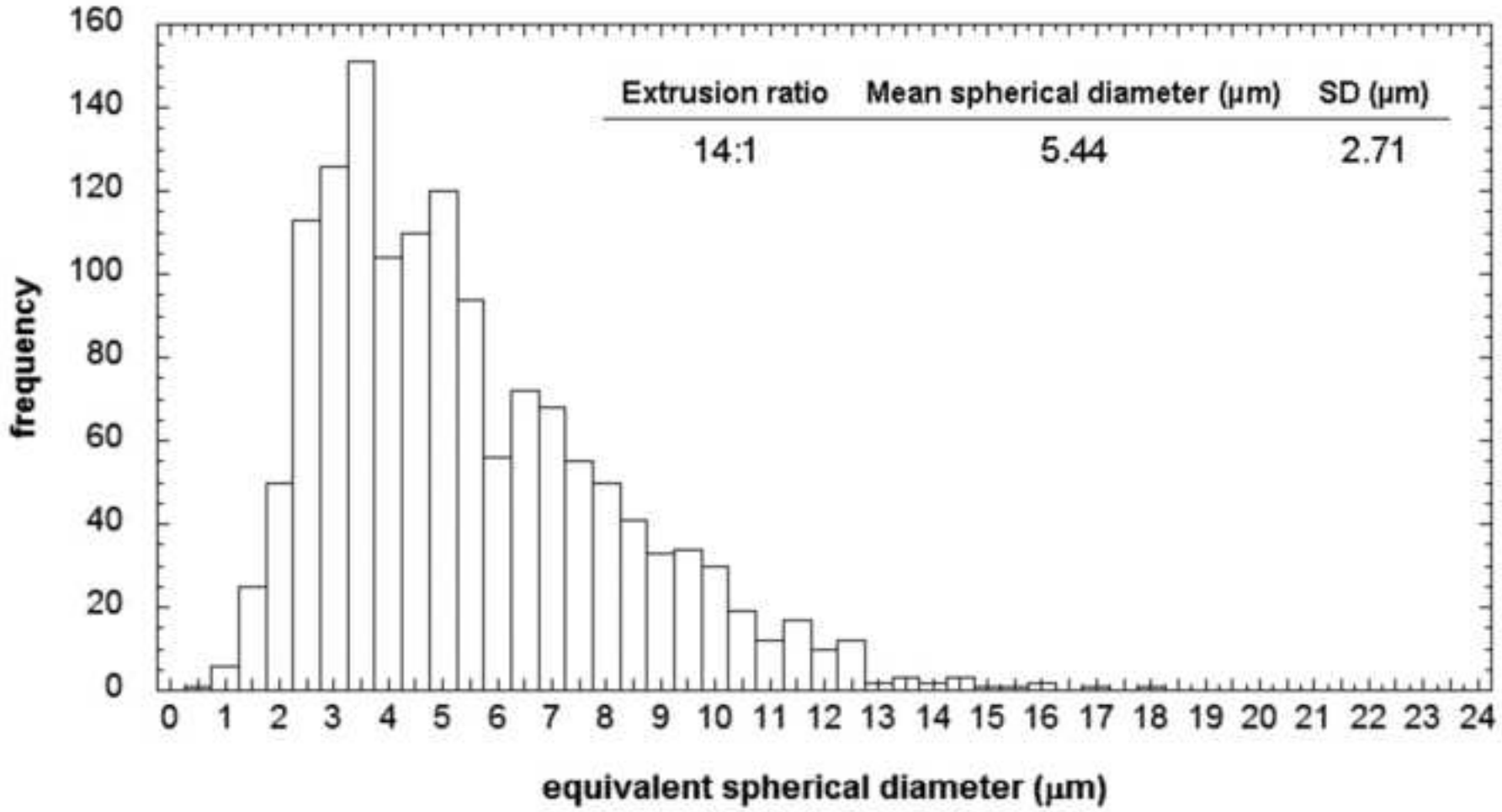

figure_07
Click here to download high resolution image

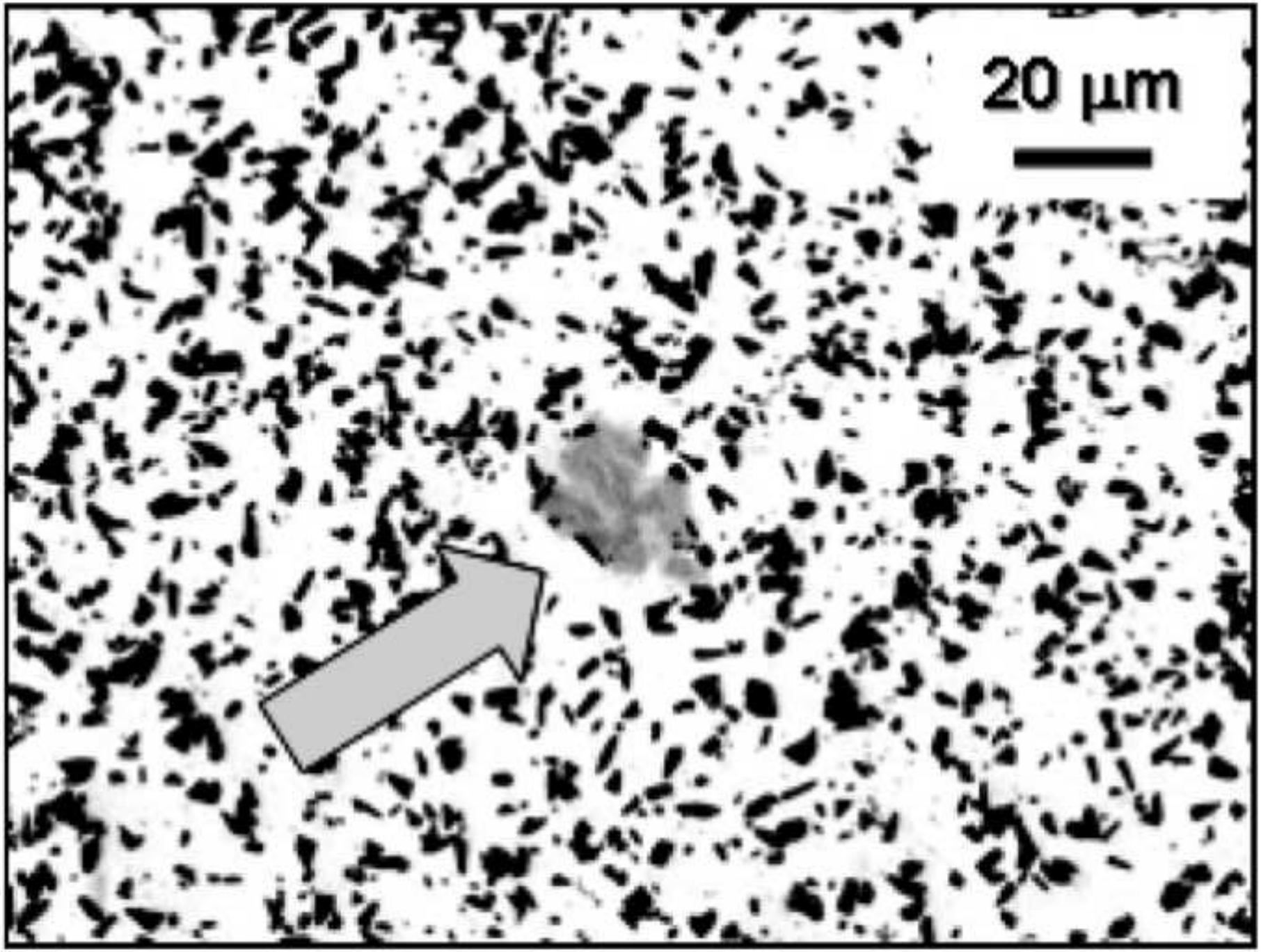

figure_08
Click here to download high resolution image

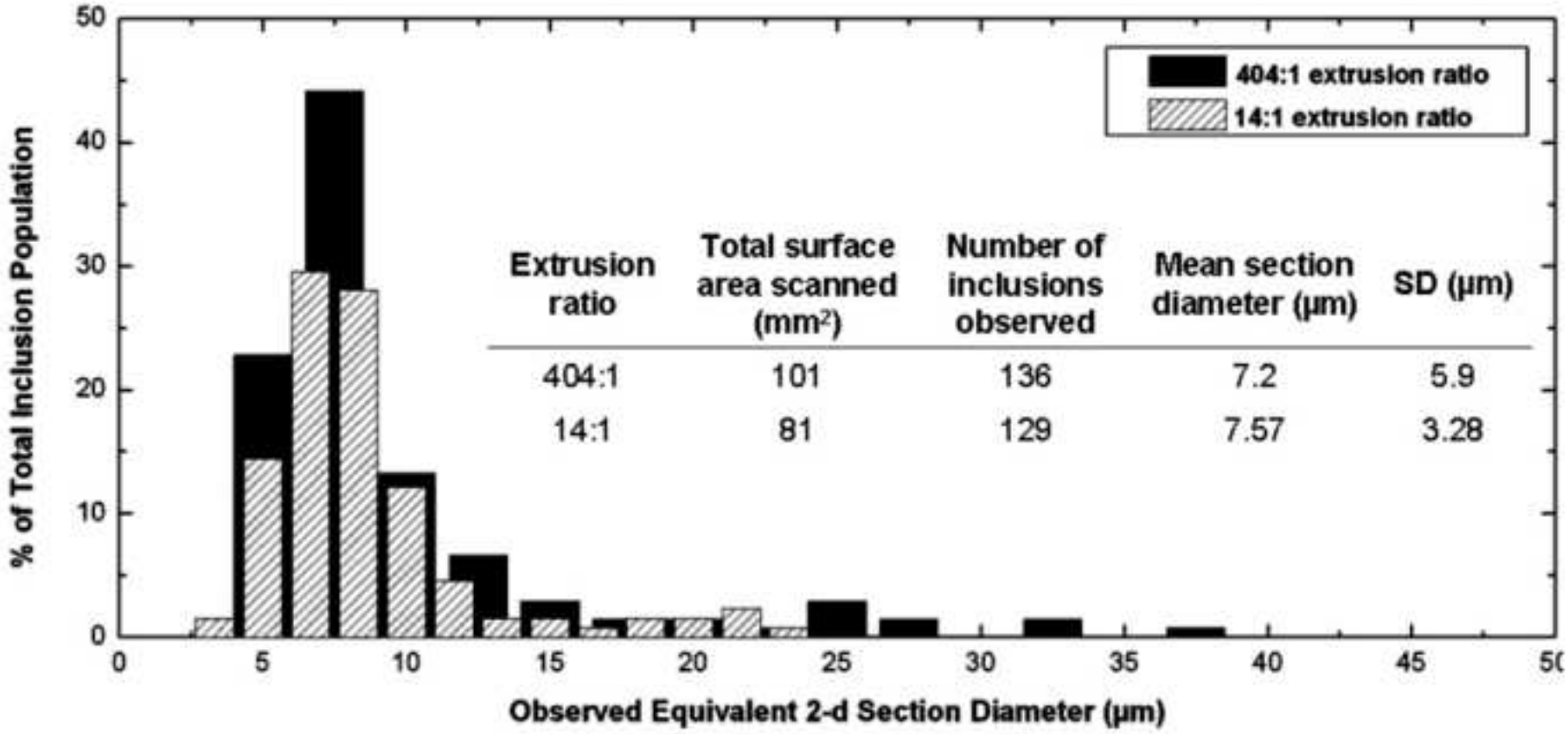

Extrusion ratio	Total surface area scanned (mm^2)	Number of inclusions observed	Mean section diameter (µm)	SD (µm)
404:1	101	136	7.2	5.9
14:1	81	129	7.57	3.28

figure_09
Click here to download high resolution image

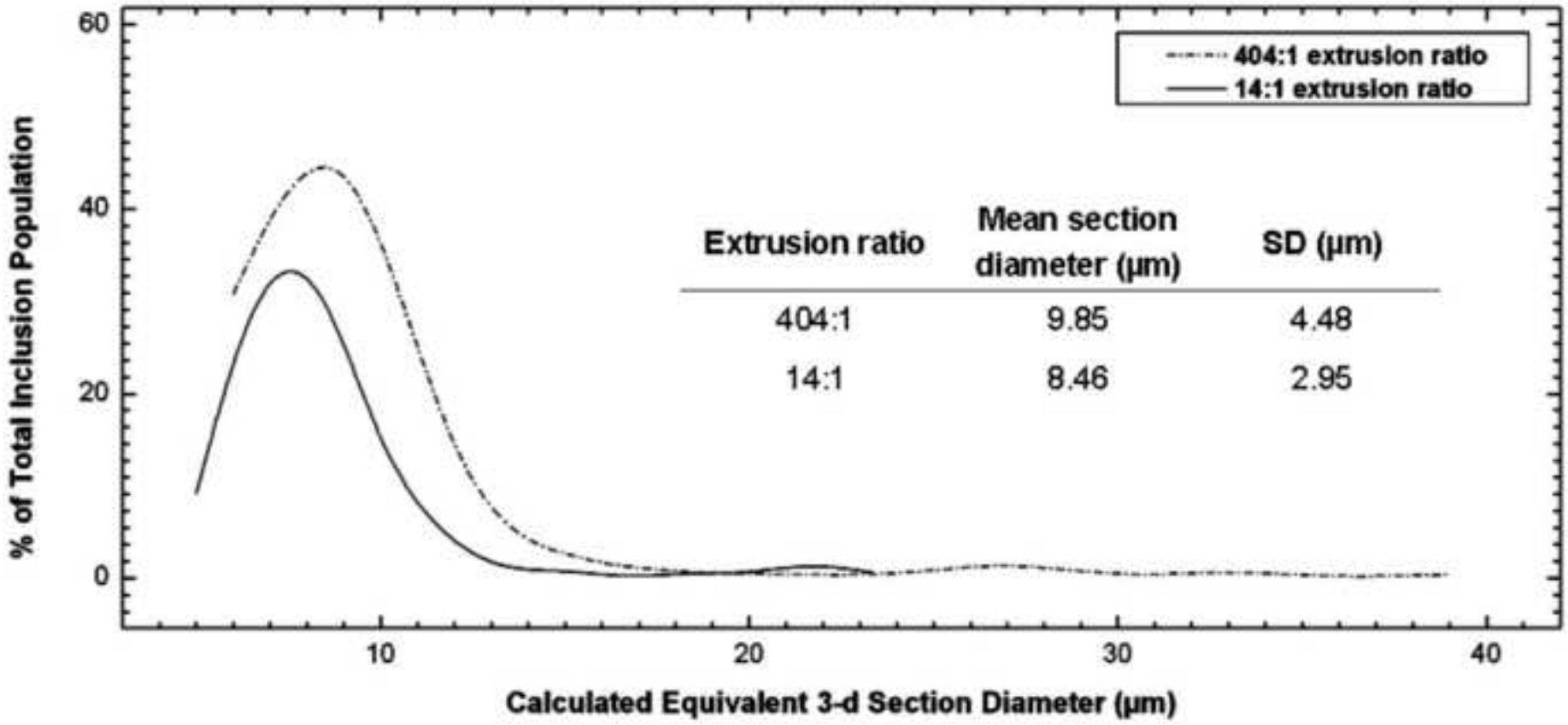

Extrusion ratio	Mean section diameter (µm)	SD (µm)
404:1	9.85	4.48
14:1	8.46	2.95

figure_10
Click here to download high resolution image

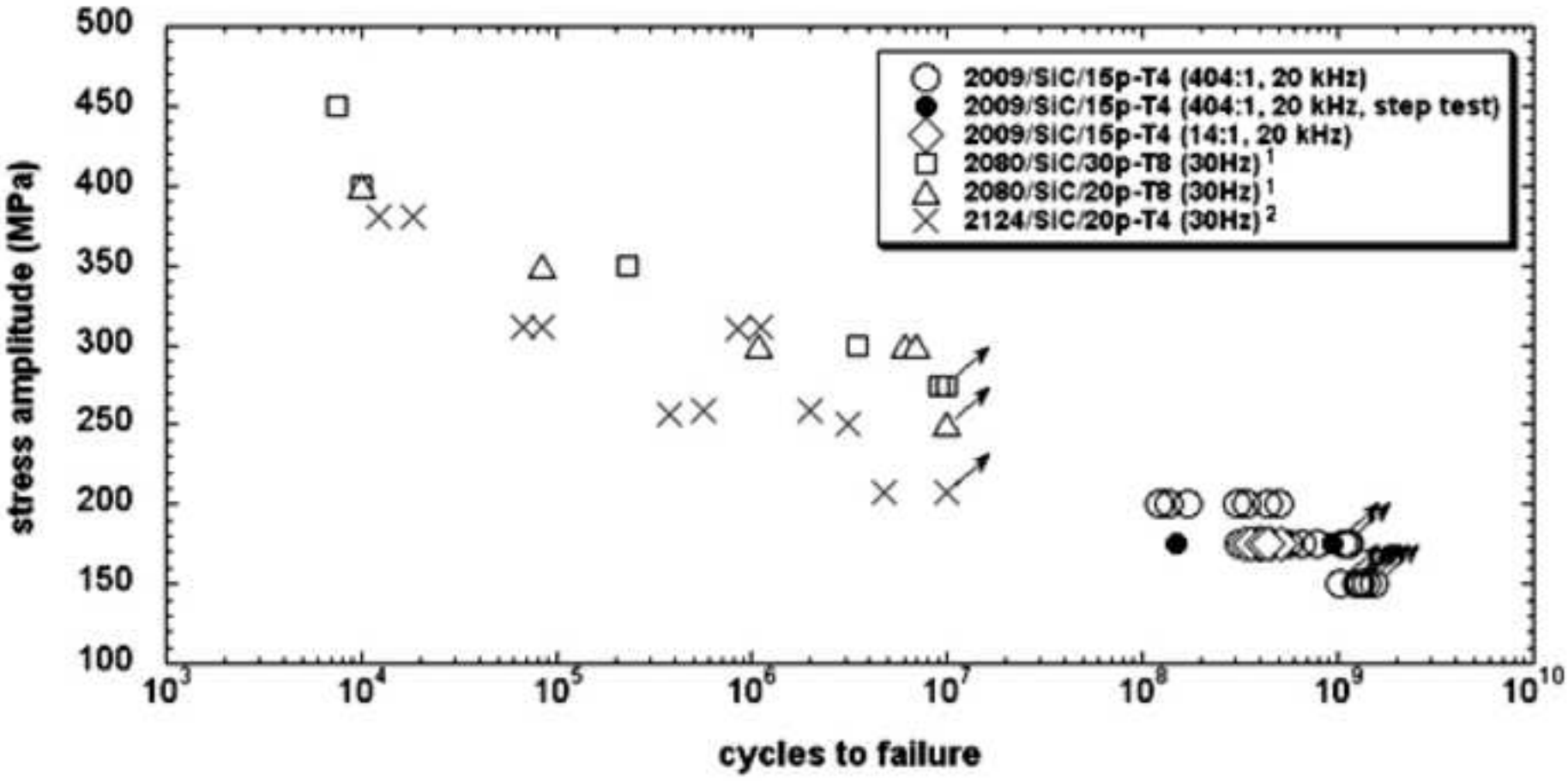

figure_11
Click here to download high resolution image

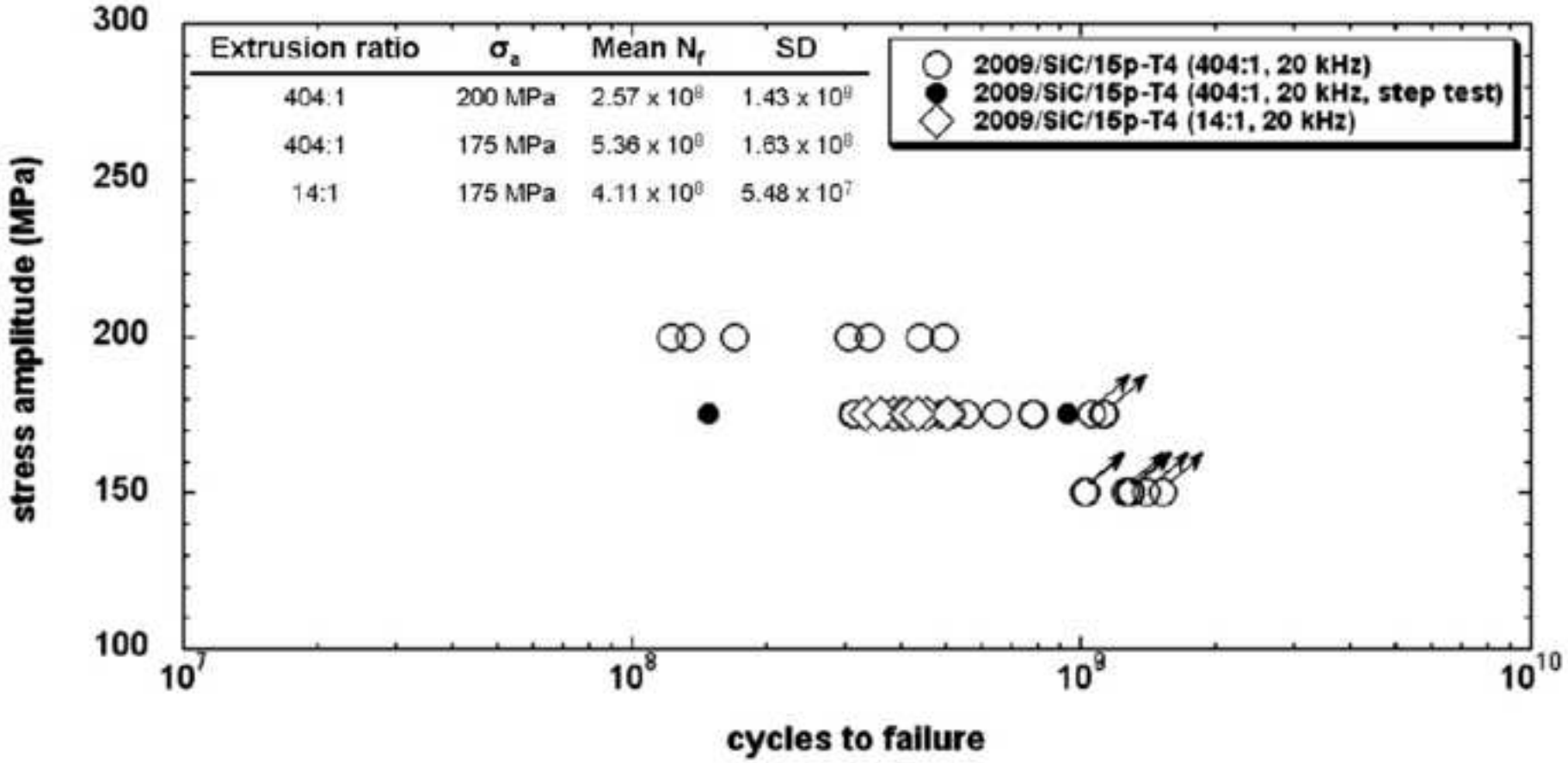

figure_12
Click here to download high resolution image

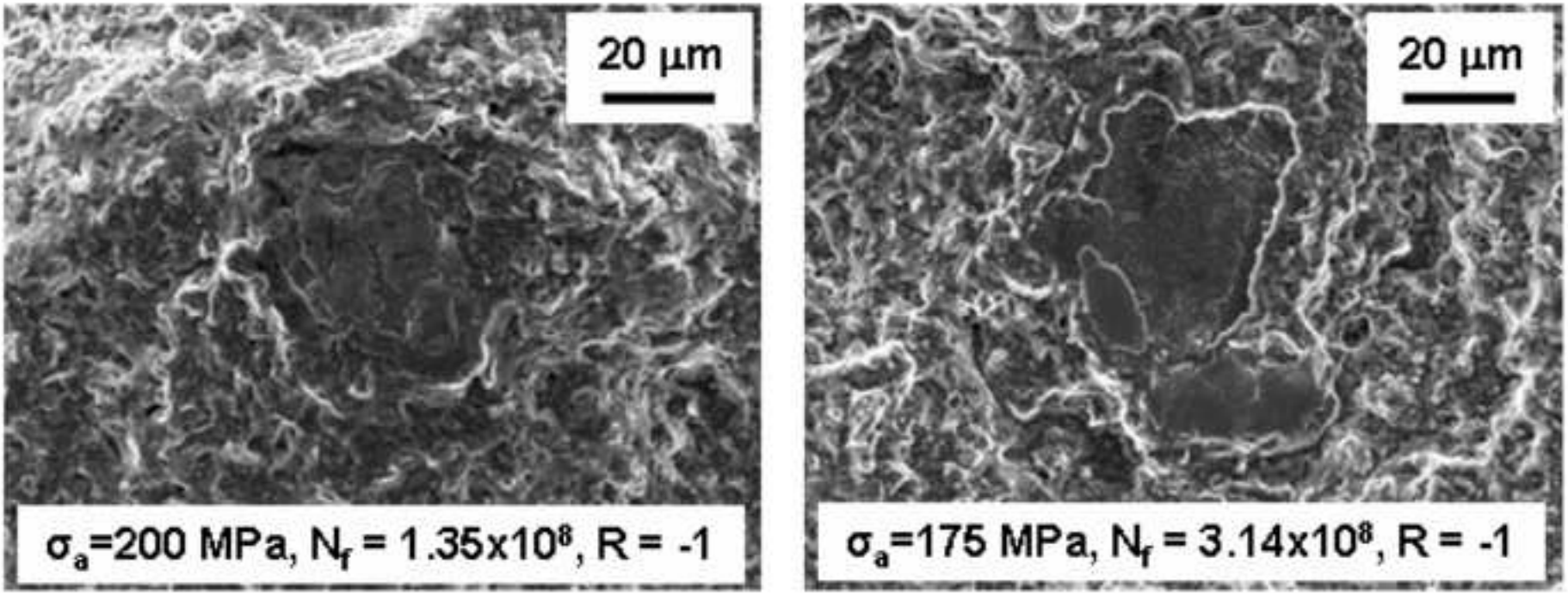

figure_13
Click here to download high resolution image

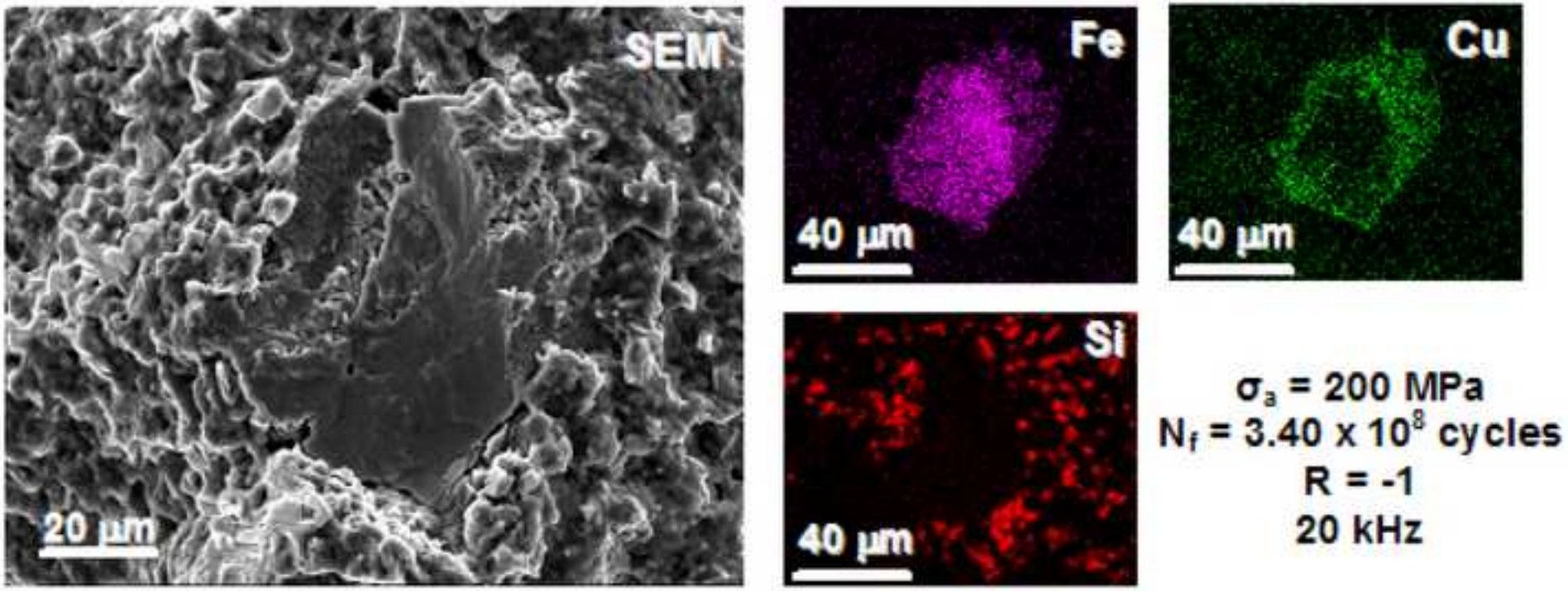

figure_14
Click here to download high resolution image

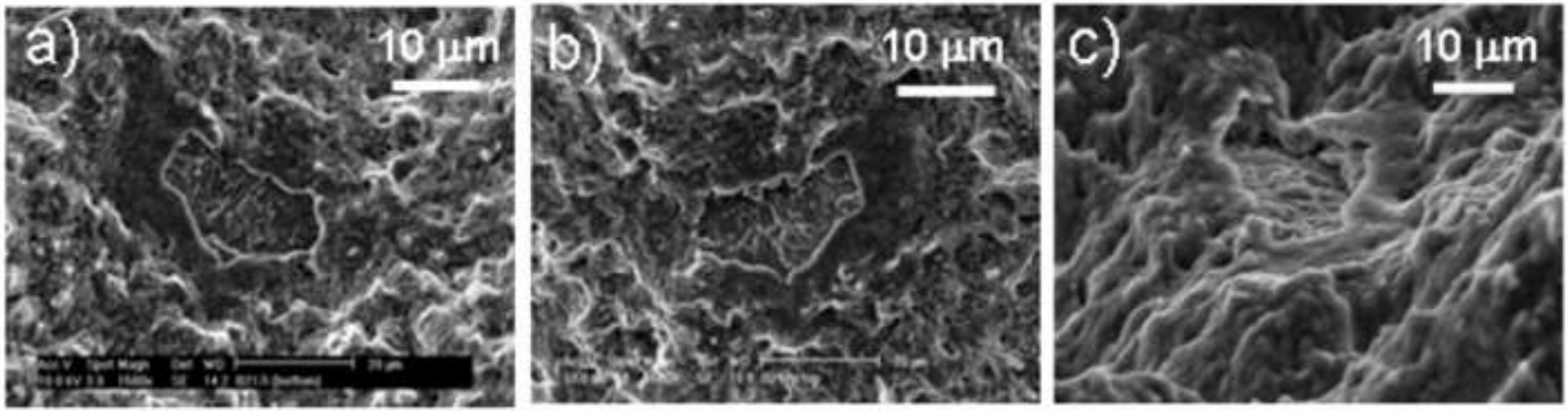

figure_15
Click here to download high resolution image

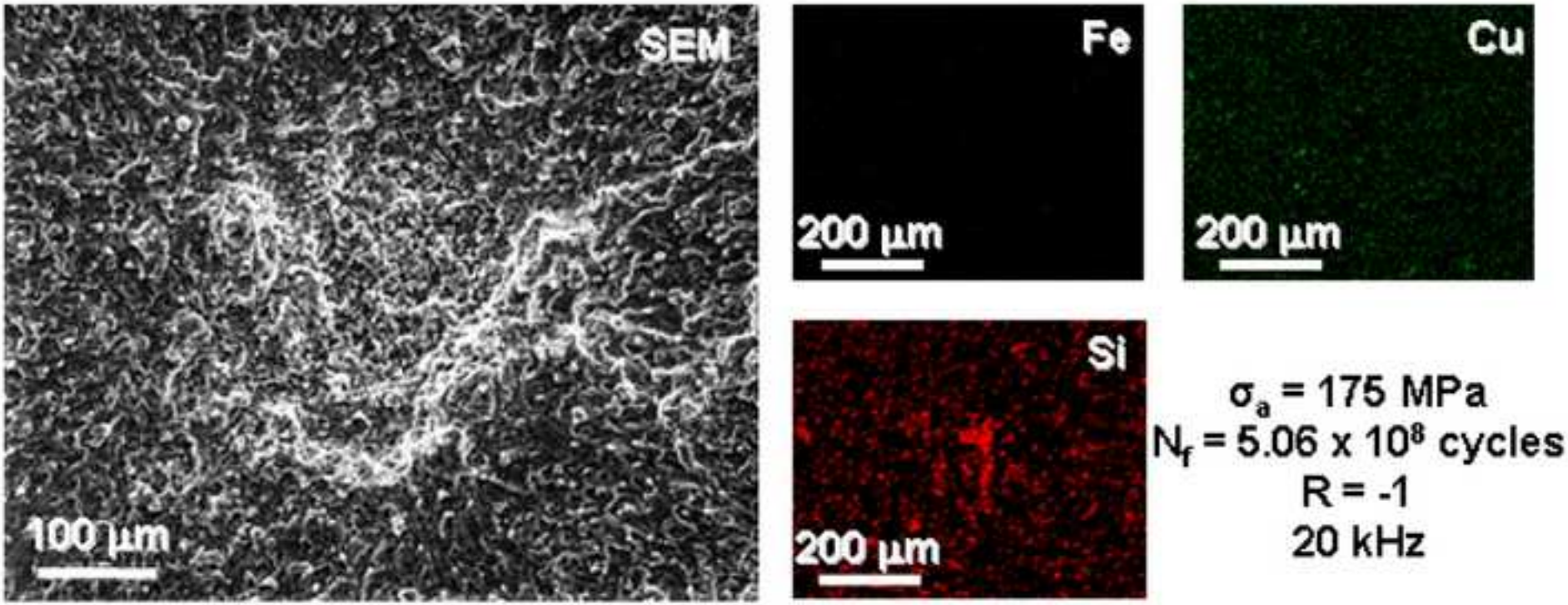

figure_16
Click here to download high resolution image

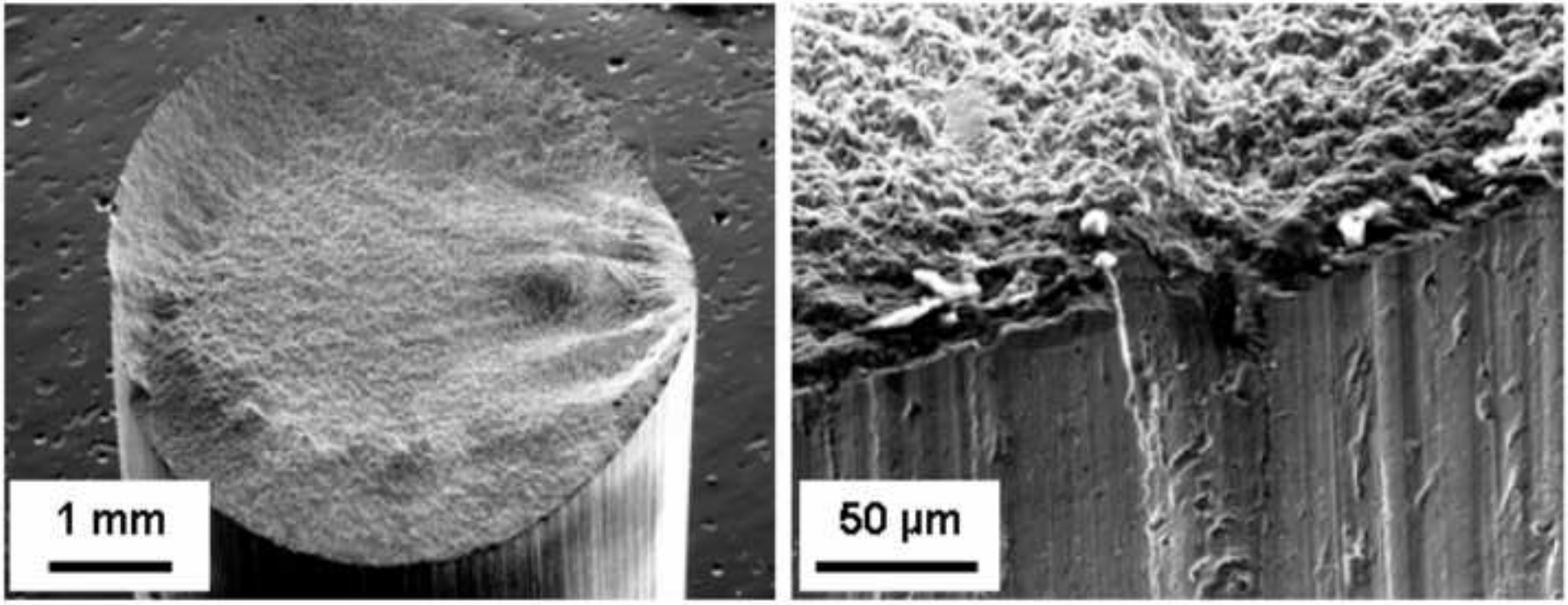

figure_17
Click here to download high resolution image

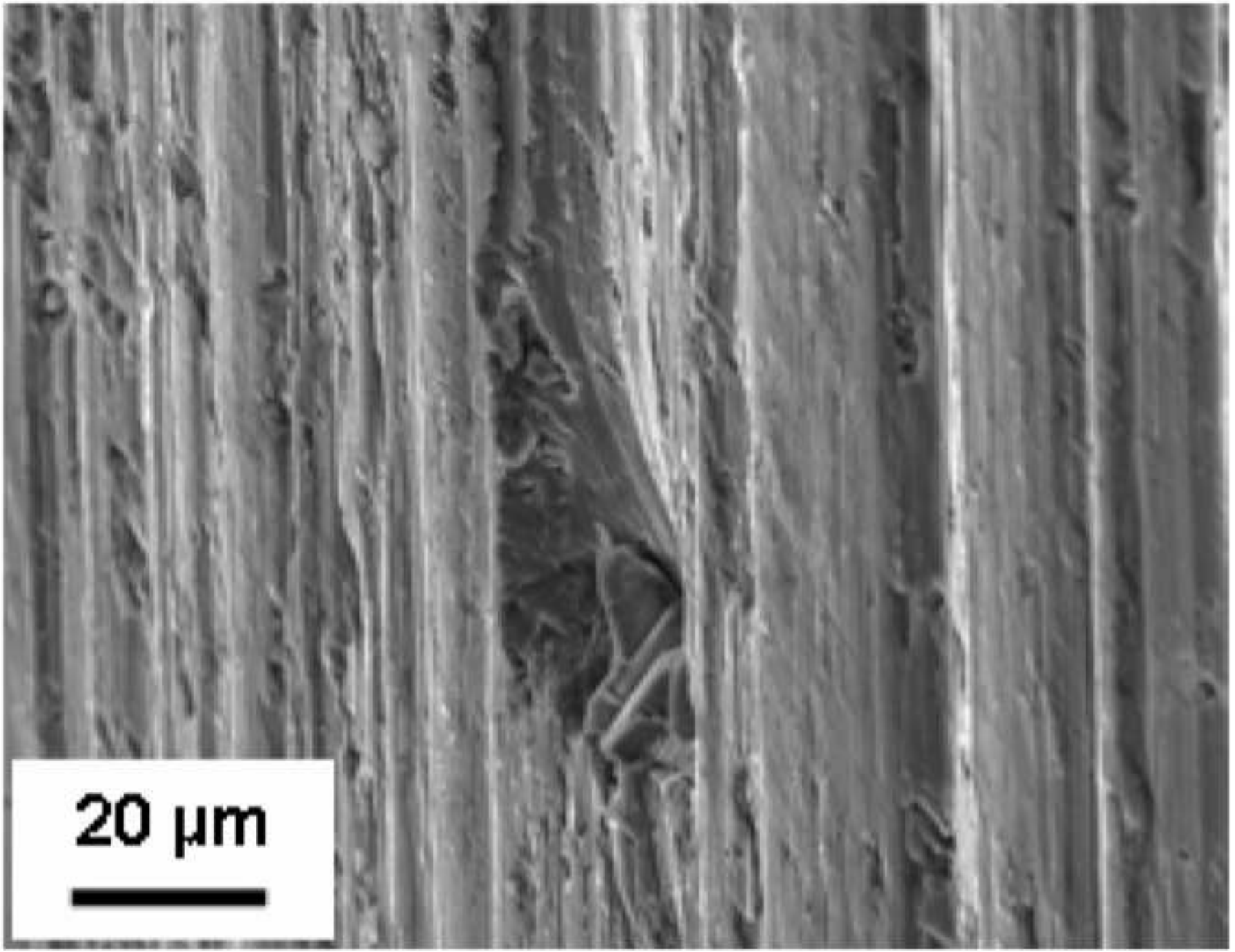

figure_18
Click here to download high resolution image

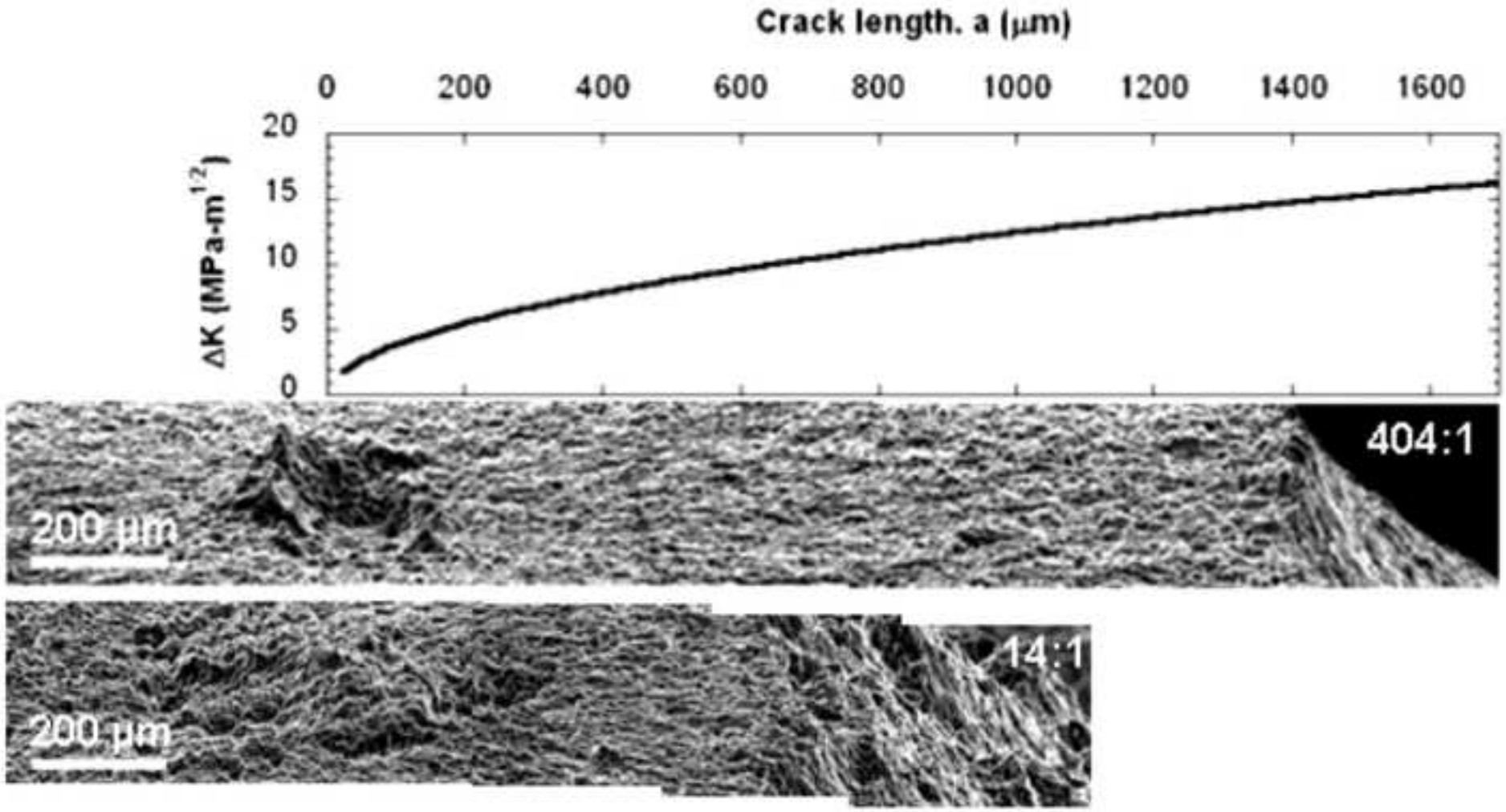

figure_19
Click here to download high resolution image

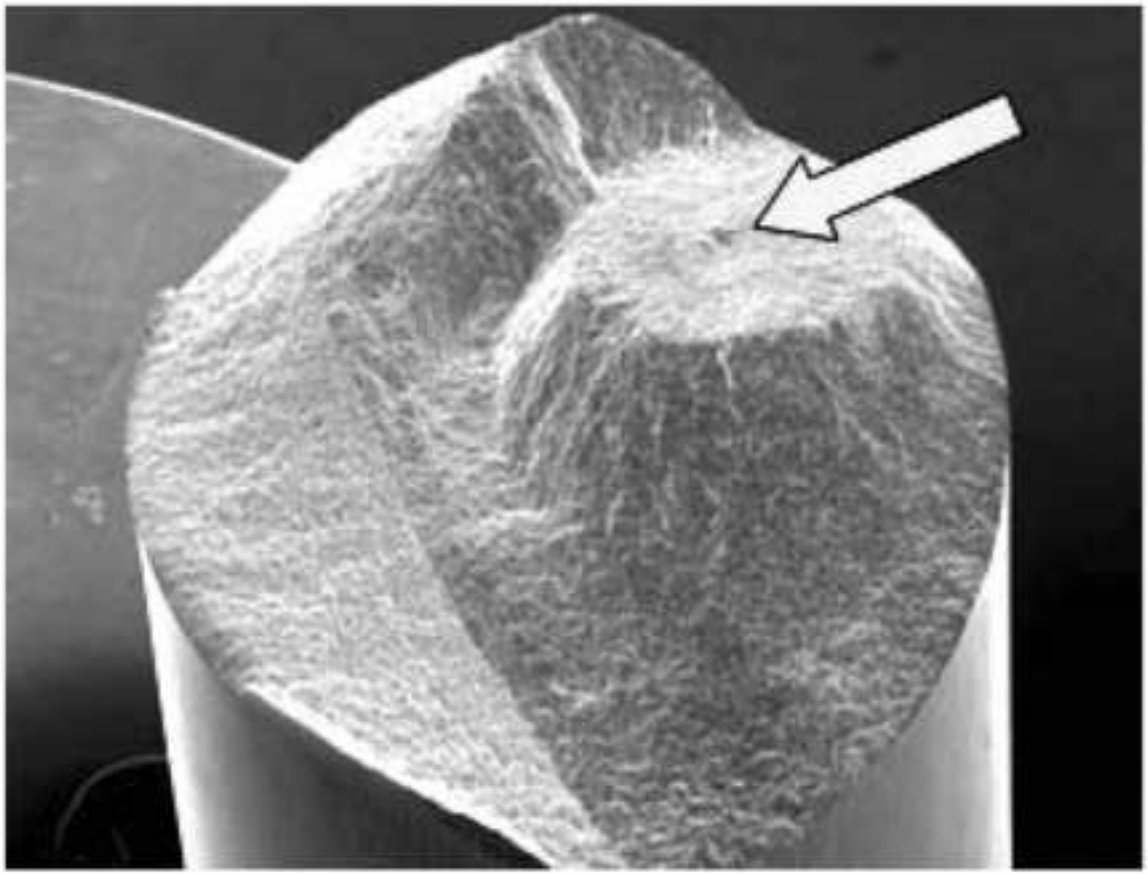

σ_a = 175 MPa
N_f = 3.76 x 10^8 cycles
R = -1
20 kHz

figure_20
Click here to download high resolution image

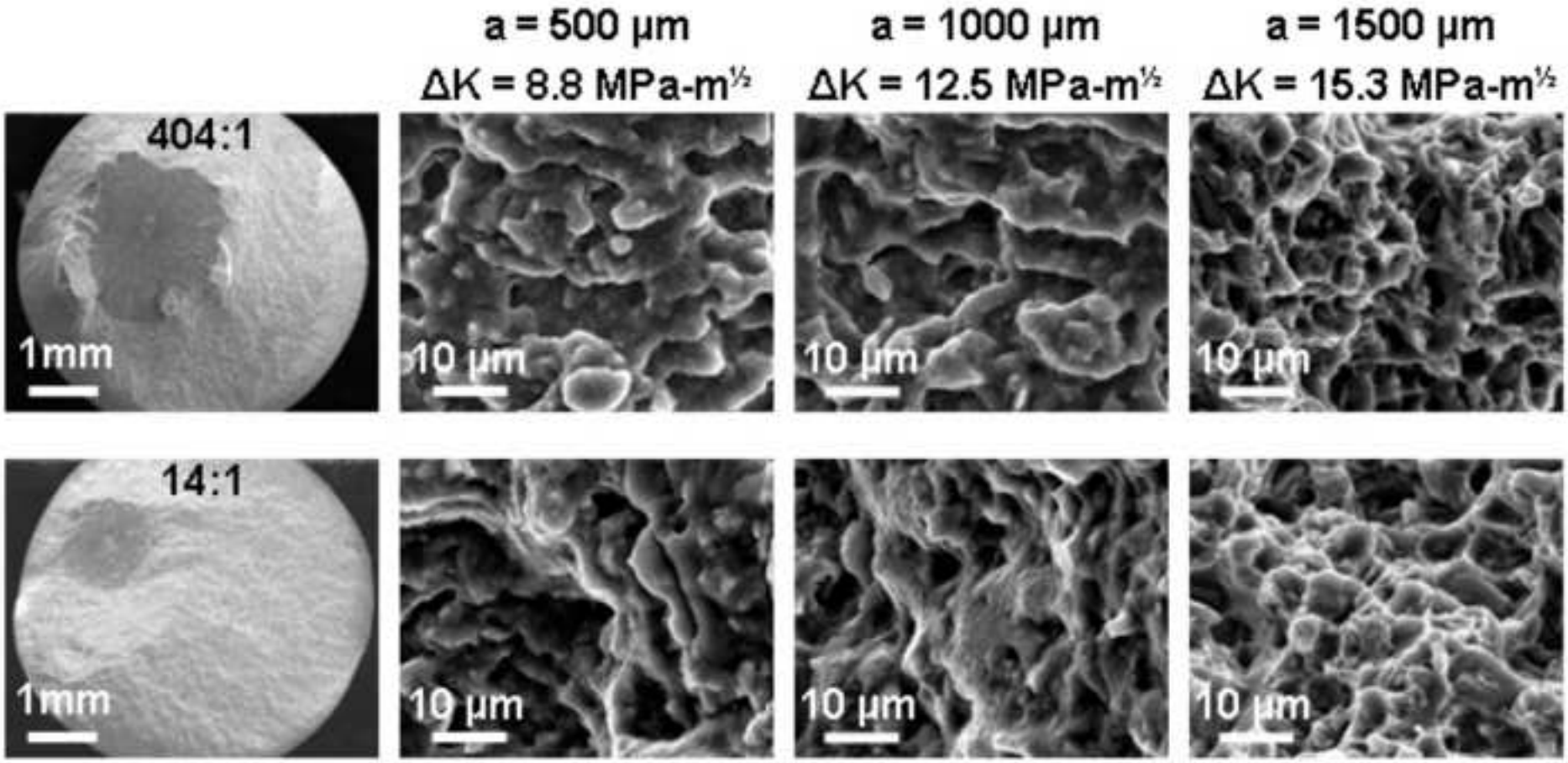

figure_21
Click here to download high resolution image